

Development and validation of a NO_x^+ ratio method for the quantitative separation of inorganic and organic nitrate aerosol using CV-UMR-ToF-ACSM

Farhan R. Nursanto¹, Douglas A. Day^{2,3}, Roy Meinen⁴, Rupert Holzinger⁴, Harald Saathoff⁵, Jinglan Fu^{5,6}, Jan Mulder⁶, Ulrike Dusek⁶, and Juliane L. Fry¹

¹Meteorology and Air Quality, Environmental Sciences Group, Wageningen University and Research, 6708PB Wageningen, the Netherlands

²Cooperative Institute for Research in Environmental Sciences, University of Colorado Boulder, Boulder, CO, USA

³Department of Chemistry, University of Colorado Boulder, Boulder, CO, USA

⁴Department of Physics, Institute for Marine and Atmospheric Research Utrecht, Utrecht University, Princetonplein 5, 3584CC Utrecht, the Netherlands

⁵Institute of Meteorology and Climate Research, Karlsruhe Institute of Technology, Eggenstein-Leopoldshafen, Karlsruhe, Germany

⁶Centre for Isotope Research, Energy and Sustainability Research Institute Groningen, University of Groningen, 9747AG Groningen, the Netherlands

Correspondence: Farhan R. Nursanto (farhan.nursanto@wur.nl) and Juliane L. Fry (juliane.fry@wur.nl)

Abstract. Particulate nitrate is a major component of ambient aerosol around the world, present in inorganic form mainly as ammonium nitrate, and also as organic nitrate. It is of increasing importance to monitor ambient particulate nitrate, a reservoir of urban nitrogen oxides that can be transported downwind and harm ecosystems. The unit-mass-resolution time-of-flight aerosol chemical speciation monitor equipped with capture vaporizer (CV-UMR-ToF-ACSM) is designed to quantitatively monitor ambient $\text{PM}_{2.5}$ composition. In this paper, we describe a method for separating the organic and ammonium nitrate components measured by CV-UMR-ToF-ACSM based on evaluating the $\text{NO}_2^+/\text{NO}^+$ ratio (NO_x^+ ratio). This method includes modifying the ACSM fragmentation table, time averaging, and data filtering. By using the measured NO_x^+ ratio of NH_4NO_3 and a plausible range of NO_x^+ ratio for organic nitrate aerosol, the measured particulate nitrate can be split into inorganic and organic fractions. Data pre-treatment filters concentrations of particulate nitrate below $0.6\text{-}2.0 \mu\text{g m}^{-3}$, depending on the time averaging. The method detection limit, when considering $\pm 10\%$ absolute uncertainty of organic nitrate fraction, is found to be $2 \mu\text{g m}^{-3}$ (120 min averaging) to $10 \mu\text{g m}^{-3}$ (10 min averaging) for total particulate nitrate concentration and 10% (120 min) to 20% (10 min) for organic nitrate fraction. We show that this method is able to distinguish periods with inorganic or organic nitrate as major components at a rural site in the Netherlands. A comparison to a high-resolution time-of-flight aerosol mass spectrometer equipped with a standard vaporizer (SV-HR-ToF-AMS) and positive matrix factorization (PMF) method shows similar response of increasing particulate organic nitrate fraction with uncertainties mainly from sensitivity to fragmentation table correction when obtaining NO_2^+ signal. We propose that researchers use this NO_x^+ ratio method for CV-UMR-ToF-ACSM (adapting the appropriate fragmentation table and data pre-treatment for each specific application) to quantify the particulate organic nitrate fraction at existing monitoring sites in order to improve understanding of nitrate formation and speciation.

1 Introduction

20 In the current age of decreasing sulfur emissions, nitrate is becoming a principal aerosol component globally and regionally (Adams et al., 1999; Metzger, 2002; Liao et al., 2003; Rodriguez and Dabdub, 2004; Feng and Penner, 2007; Bauer et al., 2007; Paulot et al., 2016; Bian et al., 2017; Vasilakos et al., 2018; Drugé et al., 2019; Lu et al., 2021). In addition to an increasing aerosol fraction of ammonium nitrate (NH_4NO_3), ambient organic nitrates (ON) produced through the oxidation of volatile organic compounds (VOCs) in the presence of nitrogen oxides (NO_x) can condense into the particulate phase or grow new
25 particles (Huang et al., 2019a, b; Song et al., 2024). The particulate ON (pON) contribution to total particulate nitrate mass (pNO_3) is substantial (Ng et al., 2017), with an average fraction of 17%-31% in China (Yu et al., 2024), 34%-44% in Europe (Kiendler-Scharr et al., 2016), and large differences between urban and rural areas (Fisher et al., 2016; Schlag et al., 2016; Romer Present et al., 2020; Yu et al., 2024). Improved understanding of pON fraction in different regions can provide insight into chemical mechanisms of secondary aerosol formation (Pye et al., 2015; Lee et al., 2016; Ng et al., 2017; Zare et al., 2018).

30 ON flux worldwide accounts $\sim 25\%$ of the total nitrogen deposition (Jickells et al., 2013). Zare et al. (2018) estimated, via WRF-Chem simulations in the southeast United States, that 60% of NO_x loss is related to ON chemistry. Similar to inorganic nitrate, ON also can be regarded as a NO_x reservoir, because thermal or photolysis processes can re-release NO_x . The partitioning between the gas-phase and particulate ON (Zare et al., 2018) can affect this reservoir lifetime, and thus the spatial scale of transport of urban nitrogen emissions from their source, determining how far downwind these emissions can
35 harm natural habitats (Fields, 2004; Bobbink and Hicks, 2014; Erisman et al., 2015; Melillo, 2021).

The NO_x^+ ratio method, first described by Farmer et al. (2010), is a robust method to separate the total pNO_3 signal measured by high resolution-aerosol mass spectrometers (AMS) into particulate ammonium nitrate (pAmN) and particulate organic nitrate (pON) using the variation of $\text{NO}_2^+/\text{NO}^+$ ion ratios (subsequently referred to as NO_x^+ ratios) in the mass spectra observed. This method has been successfully used to analyze pON composition in several studies (Fry et al., 2013; Pye et al., 2015;
40 Kiendler-Scharr et al., 2016; Ng et al., 2017; Fry et al., 2018; Huang et al., 2019a, b; Brownwood et al., 2021; Day et al., 2022a).

The basis of the NO_x^+ ratio method comes from the different fragmentation patterns of chemical species due to the interaction of the mass spectrometer's vaporizer and ionizer with the analytes. The empirical observation shows that nitrates attached to an organic moiety have different fragmentation patterns compared to nitrate in the form of NH_4NO_3 , and also other less volatile
45 inorganic nitrate. Thus, each nitrate will have different NO_x^+ ratios, R_ν , as shown below in Eq. 1 (Day et al., 2002; Francisco and Krylowski, 2005; Farmer et al., 2010; Drewnick et al., 2015; Hu et al., 2016b; Day et al., 2022a).

$$R_\nu = \frac{(C_{\text{NO}_2^+})_\nu}{(C_{\text{NO}^+})_\nu} \quad (1)$$

ν : nitrate compound or mixture measured

$C_{\text{NO}_2^+}$: signal intensity of NO_2^+

50 C_{NO^+} : signal intensity of NO^+

The NO_x^+ ratio of the observed air (R_{obs}) falls between the NO_x^+ ratios of pure pAmN (R_{pAmN}) and pure pON (R_{pON}). The time-varying mass fraction of particulate organic nitrate (f_{pON} , referring to pNO_3 existing as pON), and particulate ammonium nitrate (f_{pAmN} , referring to pNO_3 existing as pAmN) can be extracted from this time-varying R_{obs} using Eqs. 2 and 3 (Farmer et al., 2010).

$$55 \quad f_{\text{pON}} = \frac{(R_{\text{obs}} - R_{\text{pAmN}})(1 + R_{\text{pON}})}{(R_{\text{pON}} - R_{\text{pAmN}})(1 + R_{\text{obs}})} \quad (2)$$

$$f_{\text{pAmN}} = 1 - f_{\text{pON}} \quad (3)$$

The aerosol chemical speciation monitor (ACSM; Aerodyne Inc.) is a unit-mass resolution (UMR) mass spectrometry instrument intended for continuous ambient aerosol monitoring (Ng et al., 2011; Fröhlich et al., 2013), unlike its predecessor, the aerosol mass spectrometer (AMS; Aerodyne Inc.) which is designed primarily for research (Drewnick et al., 2005). In this work, we explored whether the ACSM can be used to determine pAmN and pON in the same way as has been successfully demonstrated for the AMS. ACSMs are used extensively in monitoring networks, such as the sites in the Aerosol, Clouds and Trace Gases Research Infrastructure (ACTRIS) network in Europe (<https://www.psi.ch/en/acsm-stations/overview-full-period>, last access: 6 November 2024) and the Atmospheric Science and Chemistry mEasurement NeTwork (ASCENT) network in the USA (<https://ascent.research.gatech.edu>, last access: 6 November 2024).

65 For monitoring purposes, a capture vaporizer (CV) and an intermediate pressure lens (IPL) are recommended by Aerodyne for improved quantification of the $\text{PM}_{2.5}$ fraction, relative to a standard vaporizer (SV) and standard lens (Zheng et al., 2020). Almost half of the ACSMs in the ACTRIS network in Europe use CV. The CV is designed to increase particle collision events with the vaporizer surface by having a narrow entrance, resulting in a particle collection efficiency (CE) of 1 and better mass closure of $\text{PM}_{2.5}$ monitoring (Jayne and Worsnop, 2016; Hu et al., 2017; Xu et al., 2017; Liu et al., 2024). The enhanced thermal decomposition, however, shifts the fragmentation pattern toward smaller ion fragments (Hu et al., 2017, 2018a; Xu et al., 2017; Zheng et al., 2020). Therefore, the NO_x^+ ratio is substantially lower with CV compared to SV due to favored NO^+ formation. In consequence, the NO_x^+ ratio method's applicability in CV-based measurements is limited by the NO_2^+ detection limit ($<0.1 \mu\text{g m}^{-3}$; Hu et al. (2017)).

While high resolution mass spectrometers can separate non- NO_x^+ peaks which are detected at the same nominal m/z (mass-to-charge ratio) as NO_x^+ peaks (30 for NO^+ and 46 for NO_2^+), UMR analysis requires estimations based on related ions at other m/z . These estimations are incorporated into data workup by the implementation of a fragmentation table, which subtracts an estimated amount of organic at m/z 30 and m/z 46, based on the signal at another related organic-only m/z . The default fragmentation table typically applied for the analysis of UMR spectra is based on generalized fragment mass composition of ambient aerosol composition measured using SV-based instruments (Allan et al., 2004; Ulbrich et al., 2009), and thus not suitable for CV-UMR-ToF spectra that have different fragmentation patterns. Using a CV-HR-ToF-AMS, Hu et al. (2017) determined the organic fragment interference to NO^+ in m/z 30 and to NO_2^+ in m/z 46 for CV-UMR measurements in a biogenically-dominated dataset, but no study has yet shown this calculation adapted to general ambient aerosol composition.

This work aims to adapt the NO_x^+ method to separate pAmN and pON signals to CV-UMR-ToF-ACSM measurements. We first provide a revised fragmentation table for m/z 30 and m/z 46 compatible with CV-UMR-ToF-ACSM measurements with

85 varying composition to better calculate NO^+ and NO_2^+ signal contributions. Second, we show the variation of experimental
 NO_x^+ ratio for pAmN in CV-UMR-ToF-ACSM instruments and determine the NO_x^+ ratio for pON. Third, we demonstrate the
capability of data pre-treatments (filtering and time averaging) to overcome the low and noisy ratio signals produced by CV in
ambient measurements. Fourth, the proposed NO_x^+ ratio method is applied to an extended ambient dataset (at the Cabauw site
of the Ruisdael Observatory Network) to test its robustness for changing ambient aerosol mixtures. Lastly, the formation of
90 pAmN and pON in a chamber experiment measured using CV-UMR-ToF-ACSM is used for method validation by comparing
results with SV-HR-ToF-AMS.

2 Instrumentation

2.1 Description of ToF-ACSM

A ToF-ACSM (Aerodyne Inc.) is the main instrument used in this study, allowing the chemical analysis of non-refractory or-
95 ganics (Org), ammonium (NH_4), nitrate (NO_3), sulfate (SO_4), and chloride (Chl) in the aerosol phase (Ng et al., 2011; Fröhlich
et al., 2013). In comparison to compact time-of-flight (cToF)-AMS (Drewnick et al., 2005) and HR-ToF-AMS (DeCarlo et al.,
2006), ToF-ACSM is more compact in size, lower in price and operational cost, simpler in analysis, and requires less user
intervention, which makes this instrument practical for long-term monitoring but still comparable to the AMS (Fröhlich et al.,
2013). ToF-ACSM uses a three-way valve system that allows automatic switching between the sample and filter mode, unlike
100 ToF-AMS, which has a mechanical chopper that physically blocks the particle beam. The lack of a chopper (but with the use
of particle time-of-flight chamber) in the ToF-ACSM, however, removes the particle sizing feature, which makes it similar to
the quadrupole-ACSM (Q-ACSM) but with better mass resolution and detection limits.

To conduct the various analyses in this paper, we primarily use data from two ToF-ACSM instruments with identical setup.
The instruments are managed by Utrecht University (UU) and University of Groningen (RUG), part of a larger monitoring
105 network of Ruisdael Observatory in the Netherlands (<https://ruisdael-observatory.nl>, last access: 6 November 2024). We label
the instruments as ACSM-UU and ACSM-RUG. The instrument setup for ambient measurements uses a combination of a
 $\text{PM}_{2.5}$ size-cut cyclone, an intermediate-pressure lens ($\text{PM}_{2.5}$ aerodynamic lens), and a capture vaporizer (CV, temperature
 ~ 525 °C, Jayne and Worsnop (2016)) that has been aligned with the particle beam. Together, they configure the ToF-ACSM as
a $\text{PM}_{2.5}$ monitor (Xu et al., 2017) with unit mass resolution. The instrument provides UMR mass spectra with default 10 min
110 time resolution, analyzed using Tofware v3.3 in Igor Pro 8. The fractions of the UMR signal are assigned to different aerosol
species using the fragmentation table.

2.2 Ambient measurements with ACSM

We use an ambient dataset measured using ACSM-UU deployed in Cabauw, the Netherlands, for method development and
case studies. The ambient data were measured between 18 April 2023 to 15 April 2024 with some gaps (net 205 days of
115 data) as part of the continuous monitoring of the Ruisdael Observatory network. Aerosol measurements were carried out

with an inlet height of 4.5 m above the ground at the Cabauw tower (51.97 °N, 4.93 °E), an infrastructure of the Royal Netherlands Meteorological Institute (KNMI, the Netherlands, <https://www.knmi.nl/home>, last access: 9 November 2024). The site is surrounded by agricultural lands in the province of Utrecht, the Netherlands, a relatively nitrogen-polluted rural site.

Ambient air is sampled through a stainless-steel inlet system with a PM_{2.5} size-cut cyclone (URG-2000-30ED) and a Nafion dryer with a sampling flow rate of ~ 2 L min⁻¹, of which in average 1.23 cm³ s⁻¹ (0.07 L min⁻¹) is sampled by the ACSM. The calibrations of ionization efficiency (IE) and relative IE (RIE) were performed using 300 nm particles from ammonium nitrate (NH₄NO₃) and ammonium sulfate ((NH₄)₂SO₄) solutions (size-selected with a differential mobility analyzer, model TSI 3081 and co-sampled with a condensation particle counter, model TSI 3750). The average IE value for the instrument is 169 ions pg⁻¹ for NO₃, and RIE values are 1.40, 1.58, 1.30, and 3.37 for Org, SO₄, Chl, and NH₄, respectively. RIE's used for Org and Chl were not measured, and instead applied as default values, as is common practice. The detection limits at 10 min time resolution are 0.38 μg m⁻³ for Org, 0.12 μg m⁻³ for NH₄, 0.07 μg m⁻³ for NO₃, 0.07 μg m⁻³ for NO⁺ (*m/z* 30), 0.04 μg m⁻³ for NO₂⁺ (*m/z* 46), 0.11 μg m⁻³ for SO₄, and 0.09 μg m⁻³ for Chl.

2.3 Chamber measurements with ACSM and AMS

ACSM-RUG was deployed to measure aerosol in chamber experiments conducted in Aerosol Interaction and Dynamics in the Atmosphere (AIDA) chamber, a facility maintained by Karlsruhe Institute of Technology (KIT), Germany. Chamber experiments were conducted in 2023 and 2024 as part of the Cloud-Aerosol Interactions in a Nitrogen-dominated Atmosphere (CAINA) project (<https://sites.google.com/view/cainaproject/>, last access: 6 November 2024).

Chamber air is sampled using stainless steel tubing equipped with a Nafion dryer and a sampling flow of ~ 2 L min⁻¹ of which in average 1.44 cm³ s⁻¹ (0.09 L min⁻¹) is sampled by the ACSM. The average IE value for the instrument is 152 ions pg⁻¹ for NO₃. The ACSM instrument is run with 2 min time resolution unlike the default setting to capture more variation in the aerosol composition. The detection limits at 2 min time resolution for the ACSM-RUG instrument are 0.20 μg m⁻³ for Org, 0.19 μg m⁻³ for NH₄, 0.17 μg m⁻³ for NO₃, 0.17 μg m⁻³ for NO⁺ (*m/z* 30), 0.03 μg m⁻³ for NO₂⁺ (*m/z* 46), 0.02 μg m⁻³ for SO₄, and 0.05 μg m⁻³ for Chl.

In addition, a high-resolution time-of-flight aerosol mass spectrometer (HR-AMS, Aerodyne Research Inc.) from KIT is connected to the chamber via a 6 mm (4 mm internal diameter) stainless steel tube. The instrument is equipped with a PM_{2.5} aerodynamic lens to measure the non-refractory PM_{2.5} components, at a time resolution of 1 min (DeCarlo et al., 2006; Canagaratna et al., 2007; Williams et al., 2013), averaged to 2 min for this comparison. The operation of the AMS is explained in previous publications (Huang et al., 2019a; Song et al., 2022). Briefly, chamber air is sampled with a flow of 1.08 L min⁻¹, of which in average 84 cm³ min⁻¹ is sampled by the AMS (Gao et al., 2022). The aerosol particles are then focused into a narrow beam by a PM_{2.5} aerodynamic lens with an effective complete transmission for particle sizes ranging from 70 to 2500 nm (vacuum aerodynamic diameter; D_{va}) and heated by a standard vaporizer at 600 °C. The resulting vapors are ionized by electron impact (70 eV) and characterized by a time-of-flight mass spectrometer. The AMS ionization efficiency is calibrated using 300 nm dried NH₄NO₃ aerosol particles to give an average IE NO₃ of 185.0 ions pg⁻¹. The AMS data are analysed using the software packages Squirrel 1.66E and PIKA 1.26E in Igor Pro 8. To account for the effect of particle bouncing loss,

150 chemical-composition-based collection efficiency (0.5) are applied to calculate the particle mass concentration (Middlebrook et al., 2012).

3 Development of a fragmentation table for CV-UMR-ToF-ACSM from AMS spectral database and ACSM chamber experiment spectra

3.1 General fragmentation table for typical ambient dataset

155 In the UMR-ACSM instruments, ions detected at m/z 30 and m/z 46 can originate both from nitrate (NO^+ and NO_2^+) and organic fragments. However, it is known that some fragments produced by processes in the vaporizer and ionizer can be related to one another (Allan et al., 2004). For instance, UMR peaks at m/z 29, m/z 42, m/z 43, and m/z 45 are mainly the product of further fragmentation of fragments at m/z 30 and m/z 46 and assumed to be exclusively of organic origin. The aim of the fragmentation table, with respect to the NO_x^+ species, is to predict the signal contribution of organic fragments at m/z 30 and
160 m/z 46 based on the masses measured at m/z 29, m/z 42, m/z 43, and m/z 45, and subsequently to extract the signal that can be attributed to NO^+ and NO_2^+ .

Our starting point is the default fragmentation table from Allan et al. (2004) (see Table 1). A fragmentation table consists of columns dividing the raw mass spectra into chemical species, with rows denoting entries for different UMR nominal masses. Thus, each entry consists of components which are added up to obtain the species concentration at a specific nominal mass.
165 These components can be the whole peak of an m/z x , referred to as an integer number (with square brackets in this paper, "[x "]), or the contribution of a certain species to m/z x in the fragmentation table, denoted as "frag_species[x]." A multiplier a (positive or negative) is included if the addition or subtraction of the component is fractional. The fragmentation table for ToF-AMS and ToF-ACSM are identical, except that gas-phase species contribution must also be removed in ToF-AMS. For the ACSM, due to the automatic filter sampling cycle and subtraction, gas-phase species are already removed. The fragmentation
170 table developed in this paper, therefore, is applicable to a CV-UMR aerosol mass spectrometer. Because the training data set incorporated multiple chamber and ambient measurements with different instruments, it should be applicable for a range of typical measurement configurations, but users should be aware of the potential effects of the instrument condition (e.g., vaporizer temperature, particle beam alignment, measurement history).

In the default fragmentation table (which was developed using an SV-based instrument), the signal at m/z 46 is assigned
175 exclusively to NO_2^+ , and the relationship of organic signal at m/z 30 is found to be only 0.022 times the magnitude of organic signal at m/z 29. Switching from SV to CV modifies the signal ratio between organic and inorganic fragments at m/z 30 and m/z 46, because of greater organic fragmentation in CV (Hu et al., 2018a). It also leads to greater nitrate fragmentation and consequently smaller NO_2^+ signal, which makes organic contribution at m/z 46 more important. For instance, Fry et al. (2018) found larger contributions of organic fragments at m/z 30 and m/z 46 than the default fragmentation table in a semi-polluted
180 biogenically-influenced air analyzed with an SV-HR-ToF-AMS. Therefore, modifications to frag_ NO_3 [46] and frag_ NO_3 [30] entries (later referred to as $C_{\text{NO}_2^+}$ and C_{NO^+} to calculate NO_x^+ ratio outside fragmentation table context) must be established for CV-based instruments.

Table 1. Excerpt of fragmentation table for Org and NO₃ species in m/z 30 and m/z 46. Second and third column shows entries originated from the default fragmentation table of Allan et al. (2004) (used in Tofware v3.3). Fourth and fifth column shows entries proposed to develop revised CV-UMR-ToF-ACSM fragmentation table in this study.

m/z	Allan et al. (2004), default fragmentation table		Proposed for general CV-ToF-ACSM	
	Org	NO ₃	Org	NO ₃
30	0.022 · frag_Org[29]	[30], -frag_Org[30]	$a_{\text{Org}[30],[i]} \cdot \text{frag_Org}[i]$ ^(a)	[30], -frag_Org[30]
46	-	[46]	$a_{\text{Org}[46],[i]} \cdot \text{frag_Org}[i]$ ^(b)	[46], -frag_Org[46]

i represents UMR masses tested against m/z 30 and m/z 46 in this study, which includes frag_Org[29], frag_Org[42], frag_Org[43], and frag_Org[45]. See the list in the footnote of Table S3 of SI.

(a) $a_{\text{Org}[30],[i]}$ is the multiplier for frag_Org[30] component, obtained from the slope of ODR fit between frag_Org[30] and frag_Org[i].

(b) $a_{\text{Org}[46],[i]}$ is the multiplier for frag_Org[46] component, obtained from the slope of ODR fit between frag_Org[46] and frag_Org[i].

To make a revised fragmentation table applicable for general ambient organic aerosol (OA) mixtures, a variety of organic aerosol profiles is necessary. We use 25 CV-HR-ToF-AMS spectra (including both nitrates and non-nitrate organics) from the AMS spectral database (http://cires1.colorado.edu/jimenez-group/AMSsd_CV, last access: 6 November 2024) and 6 CV-UMR-ToF-ACSM spectra from chamber experiments. The CV-HR-ToF-AMS database mass spectra include 3 chamber experiments, 7 factors of positive matrix factorization (PMF) analysis from ambient measurements, and 15 laboratory standards measurements (Hu et al., 2017; Carlton et al., 2018; Hu et al., 2018a, b), summarized in Table S1 in the Supplementary Information (SI). The CV-UMR-ToF-ACSM mass spectra were measured from experiments conducted in the AIDA chamber (see Section 2.3). These spectra were obtained using vaporizer temperature ranging from 525 to 600 °C (see Table S1 and S2). Therefore, the revised fragmentation table should be valid for CV-based instruments run in this temperature range.

Using these data, we determine the multipliers a used in a revised calculation of frag_Org[30] and frag_Org[46] (see Table 1, fourth and fifth column and Table S1, third and fourth column). The new multipliers are determined by performing orthogonal distance regression (ODR) constrained to a zero intercept of mass spectra in UMR. For HR-AMS spectra, the dataset is "degraded" from HR into UMR spectra by summing HR Org fragments to their respective nominal mass in each AMS spectrum. Note that for UMR-ACSM spectra, because we cannot separate species at the same nominal m/z , we only use chamber experiments that are assumed nitrate-free or to contain negligible nitrate (no seed or precursor for inorganic and organic nitrate). Therefore, all signals at m/z 30 and m/z 46 are exclusively organic fragments. We perform ODR fits of frag_Org[30] and frag_Org[46] against a list of chemically related masses (frag_Org[i]). The slope of the ODR fits to determine the multiplier $a_{\text{Org}[30],[i]}$ and $a_{\text{Org}[46],[i]}$ are summarized in Table S3, alongside the list of fragments of i that contribute to each nominal mass, in the footnote. It is found that frag_Org[30] is best correlated with frag_Org[29] (see Table S3), where $a_{\text{Org}[30],[29]} = 0.311 \pm 0.016$ (mean \pm uncertainty, $r^2 = 0.88$, see Fig. 1a). On the other hand, frag_Org[46] has the best correlation with frag_Org[45] (see Table S3), where $a_{\text{Org}[46],[45]} = 0.305 \pm 0.037$ (mean \pm uncertainty, $r^2 = 0.43$, see Fig. 1b). The final revised fragmentation table in CV-UMR-ToF-ACSM is summarized in the conclusions (see Table 4).

We apply these new multiplier values to the full dataset and compare the results with those from multipliers described in Allan et al. (2004), the SI of Fry et al. (2018), and the SI of Hu et al. (2017) (see in Table S4). The result suggests that the

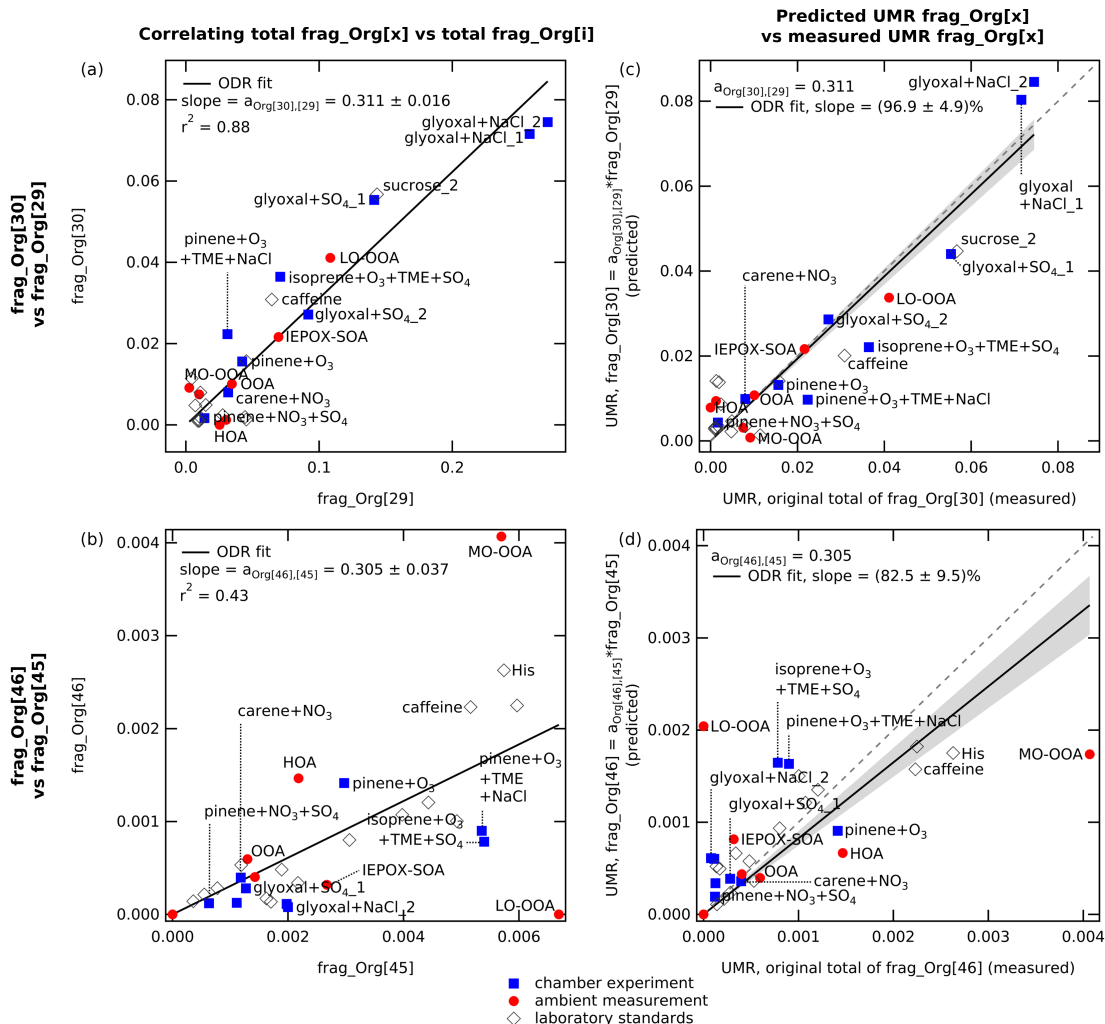


Figure 1. The left-hand panels show the best ODR fits (set to zero intercept) which are found in the relationship between the signal contributions of (a) frag_Org[30] vs frag_Org[29], and (b) frag_Org[46] vs frag_Org[45]. The correlations of all mass pairs are summarized in Table S3. The right-hand panels show the predicted organic contributions (based on the new multipliers) at each m/z versus the measured amount. Plot (c) shows the predicted UMR frag_Org[30] against the measured total Org fragments in m/z 30, and plot (d) shows the predicted UMR frag_Org[46] against the measured total Org fragments in m/z 46. The figure demonstrates that the predicted frag_Org[x] slightly underestimates (slope = 0.83) but approached the measured frag_Org[x].

multiplier $a_{\text{Org}[46],[45]}$ determined here gives the best predicted frag_Org[46] over multipliers from other studies (see Table S4 third and seventh columns in the SI). Meanwhile, the multiplier $a_{\text{Org}[30],[29]}$ determined here performs similarly with the multipliers obtained from Hu et al. (2017) (SV and CV) for a dataset dominated by biogenic secondary organic aerosol (SOA).

210 The plot of predicted UMR frag_Org[30] against the measured total Org fragments in m/z 30 (see Fig. 1c) shows that the

multiplier determined here is able to estimate on average $96.9 \pm 4.9\%$ of the measured frag_Org[30]. Meanwhile, the similar plot for frag_Org[46] against the measured total Org fragments in m/z 46 (see Fig. 1d) shows that the multiplier determined here estimates on average $82.5 \pm 9.5\%$ of the measured frag_Org[46]. The low signal intensity of both m/z 46 and m/z 45 may cause this underestimation and suggests that frag_Org[46] and frag_Org[45] may have a more complicated relationship; their correlation may vary substantially depending on the aerosol mixture. Therefore, it may be appropriate to modify the entry for frag_NO₃[46] according to the type of aerosol mixture analyzed. On the other hand, for complex ambient mixtures, the ensemble composition may produce spectra that are more similar to the average determined here. Analysis of CV-HR spectra from a variety of ambient samples would be required to determine the actual variation of organic contributions at m/z 46.

3.2 Composition-specific fragmentation table

The multipliers determined in Section 3.1 are designated for typical ambient aerosol composition. In some cases, a composition-specific fragmentation table may be more appropriate to use. For instance, from a field study with biogenically-dominated composition, Hu et al. (2017) reported $a_{\text{Org}[30],[29]} = 0.32$ and $a_{\text{Org}[46],[45]} = 0.68$. By using selected chamber experiments in the same dataset, we can explore different multipliers that are compatible for different composition profiles. For chamber experiments that involves glyoxal (and its oligomers), we obtain $a_{\text{Org}[30],[29]} = 0.291 \pm 0.022$ (mean \pm uncertainty, $n = 4$, $r^2 = 0.90$) and $a_{\text{Org}[46],[45]} = 0.082 \pm 0.036$ (mean \pm standard deviation, $n = 4$, $r^2 = 0.35$). For chamber experiments that involve only terpenes (e.g., isoprene, α -pinene), we obtain $a_{\text{Org}[30],[29]} = 0.476 \pm 0.067$ (mean \pm uncertainty, $n = 5$, $r^2 = 0.82$) and $a_{\text{Org}[46],[45]} = 0.204 \pm 0.055$ (mean \pm uncertainty, $n = 5$, $r^2 = 0.33$) which can be applied for chamber experiments with terpene as precursor. The ODR fit plots are given in Fig. S1. The multipliers to revise the fragmentation table in CV-UMR-ToF-ACSM for specific aerosol composition subsets is summarized in the conclusions (see Table 4).

4 Determination of NO_x⁺ ratios for the CV-UMR-ToF-ACSM

4.1 NO_x⁺ ratio of pure pAmN

To quantify the inorganic NO_x⁺ ratio typical value and variability produced by the CV, we use repeated measurements from regular pAmN calibration from the two ACSM instruments described in Section 2. The R_{pAmN} of ACSM-UU is found to be 0.0237 ± 0.0009 (mean \pm uncertainty, $n = 5$), and R_{pAmN} of ACSM-RUG is 0.0115 ± 0.0002 (mean \pm uncertainty, $n = 3$). The values are similar but lower than other studies where R_{pAmN} with CV was found to be 0.04-0.07 (Hu et al., 2016a), and all are ~ 10 times lower than the typical R_{pAmN} measured with the SV, 0.3-0.7 (Day et al., 2022b). We found that R_{pAmN} values are very consistent for each instrument over time. A summary of R_{pAmN} values and regression fit parameters from each measurement can be found in Table S5 in the SI.

Hu et al. (2017) found that the NO_x⁺ ratio is affected by the aerodynamic lens alignment. The influence is greater in the CV since the vaporizer opening diameter is ~ 2.5 mm (SI of Hu et al. (2018b)), smaller than that of SV, which is ~ 3.8 mm (Drewnick et al., 2005). For optimum particle detection, the aerodynamic lens must point the particle beam at the center of

the vaporizer. Directed into the center, the particles enter the CV cavity and experience augmented thermal decomposition, at which the NO_2^+ signal intensity is at its minimum, while the NO^+ signal intensity is highest. The NO_2^+ signal intensity increases as the particle beam moves closer to the edge of the vaporizer, where the thermal decomposition is not as extensive as in the center, resembling how the SV works. Thus, it is important to consider performing lens alignment to obtain the correct result for the NO_x^+ ratio method. Monitoring the behavior of m/z 30 and m/z 46 in during pAmN calibration is a good way to determine whether the aerodynamic lens is well aligned. Combining the result of this study and the R_{pAmN} range in Hu et al. (2017), value of R_{pAmN} in the range of 0.01-0.07 can be used as reference to indicate properly aligned lens. Plotting the profile of the NO_x^+ ratio with movement in both the vertical and horizontal directions obtained during the alignment is the best diagnostic.

4.2 NO_x^+ ratio of pure pON

To obtain a NO_x^+ ratio for pON, one would ideally measure pure atmospherically-relevant ON, prepared through synthesis or in a chamber experiment. Often, such standards are not available and therefore experimental R_{pON} cannot be easily determined for each instrument. To overcome this challenge, Day et al. (2022a) used the strategy of a "ratio-of-ratios" ($RoR = R_{\text{pAmN}}/R_{\text{pON}}$) which can be used to calculate R_{pON} for any arbitrary instrument from its routinely-measured R_{pAmN} , and an average value for the RoR measured across many instruments under varying conditions. Day et al. (2022a) found that based on the relationship between R_{pAmN} and R_{pON} over a large range of measurement conditions, SV produces RoR of 2.75 ± 0.70 (mean \pm 25% uncertainty).

There have not been enough studies yet that have determined R_{pON} values in CV-based instruments in order to determine a robust RoR estimate for CV instruments. In the work of Hu et al. (2017), a chamber experiment producing pure pON yielded $R_{\text{pON}} = 0.0045$, and with comparison to $R_{\text{pAmN}} = 0.06$ of their instrument, the value $RoR = 13.3$ is obtained. With R_{pAmN} being 0.01 in CV as found in this study, using this RoR of 13.3, R_{pON} would be 0.0008 (approaching zero).

Similar to the approach of Kiendler-Scharr et al. (2016) that used the minimum measured value of NO_x^+ ratio to set a fixed R_{pON} value, to estimate R_{pON} , we use the lowest measured NO_x^+ ratio from a chamber experiment in which we expected to produce pON, with no inorganic nitrate present. The selected experiment used glyoxal as SOA precursor, NO_2 and O_3 to produce NO_3 radical as the major oxidant, and sodium chloride (NaCl) seed to form SOA containing organic nitrates at 90% relative humidity. This experiment was conducted in the AIDA chamber at IMK KIT, Germany as part of CAINA project. For the spectra analysis, we use the fragmentation table specific for glyoxal-related chamber experiment, as described in Section 3.2.

While this experiment should produce pure organic nitrate aerosol, during pON formation, we observe an increase in NH_4 which could happen for two reasons. First, ammonium nitrate impurities can be formed from reactions or chamber wall re-partitioning. Second, particulate water can be incorrectly assigned as NH_4 through fragmentation table correction at the m/z 16 and m/z 17 (see complete fragmentation table in Allan et al. (2004)). Both can result in a higher NO_x^+ ratio than as we would have if the total nitrate were purely pON. Therefore, we derive two bounding R_{pON} values from the glyoxal chamber experiment. First, we determine the R_{pON} from the experiment by assuming pure pON formation to obtain an upper limit. Second, to

obtain the lower limit of R_{pON} , we assume all observed NH_4 increase is NH_4NO_3 aerosol and subtract this equivalent amount of inorganic nitrate, with the inorganic NO_x^+ ratio, from the total NO_3 , in order to obtain a lower limit of pON time series and calculate the R_{pON} . This strategy has been described as the "excess NH_4 " method in Takeuchi and Ng (2019). By rearranging the Eq. 2 to Eq. S2, we can obtain R_{pON} using f_{pON} , R_{pAmN} , and R_{obs} for the lower limit experiment (see details in Section S3 of SI).

The upper limit experiment gives $R_{\text{pON}} = 0.0035$ (see Fig. 2a). If we compare to $R_{\text{pAmN}} = 0.0115 \pm 0.0002$ (measured separately with pure AmN), $R_{\text{pON}} = 0.0035$ obtained from the upper limit experiment gives $RoR = 3.29$ (see Fig. 2a). This value is higher than RoR for SV-AMS but lower than RoR obtained from Hu et al. (2017).

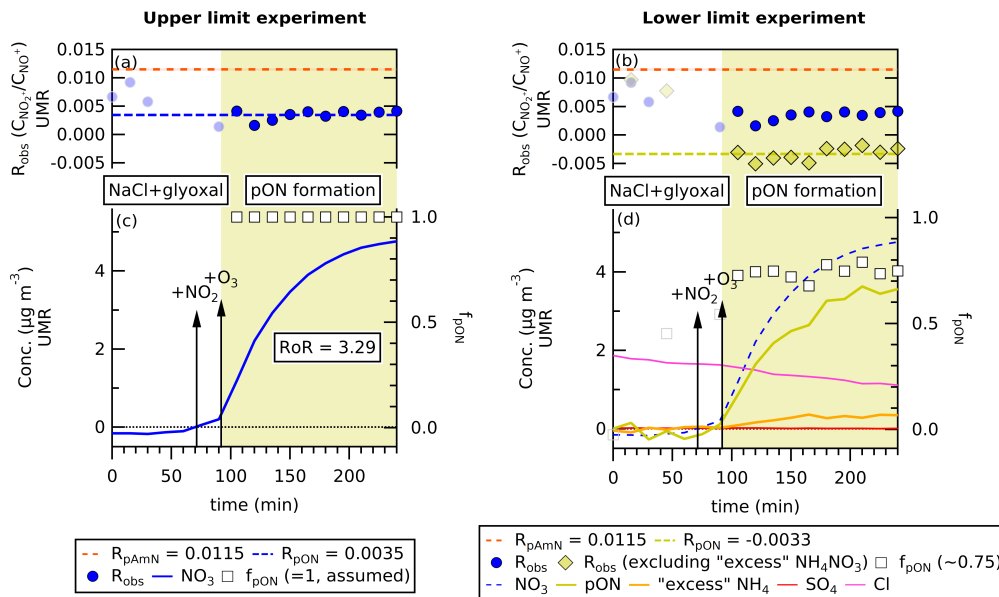


Figure 2. The time series of (a and b) R_{obs} , (c and d) ACSM species concentration (in $\mu\text{g m}^{-3}$, left bottom axis), and f_{pON} (right bottom axis) of glyoxal+ NO_3 chamber experiment at 15 min time averaging. The UMR fragmentation table specific for glyoxal is used to obtain $C_{\text{NO}_2^+}$ and $C_{\text{NO}_2^+}$. Panels (c) and (d) shows the progression of NO_3 concentration, compared to panels (a) and (b) for the NO_x^+ ratio during the formation of pON. By averaging R_{obs} after pON formation started, the left-hand panel shows that $R_{\text{pON}} = 0.0035$ is obtained when assuming $f_{\text{pON}} = 1$. When possible inorganic impurity is removed by assuming “excess” NH_4 are NH_4NO_3 , the average f_{pON} is found to be 0.75. The excess NH_4 concentration is obtained by subtracting total NH_4 concentration by the average NH_4 concentration before the addition of NO_2 and O_3 (to exclude any possible NH_4Cl contribution). By calculating R_{pON} using the obtained f_{pON} from “excess NH_4 ” method, R_{pAmN} and R_{obs} , the value $R_{\text{pON}} = -0.0033$ is obtained, suggesting an overcorrection (see text). The value $R_{\text{pON}} = 0.0035$ from the lower limit experiment and $R_{\text{pAmN}} = 0.0115 \pm 0.0002$ (mean \pm uncertainty) give a ratio-of-ratios ($RoR = R_{\text{pAmN}}/R_{\text{pON}}$) of 3.29.

On the other hand, the lower limit experiment gives $R_{\text{pON}} = -0.0033$ (see Fig. 2b). A negative (or below zero) R_{pON} value is not chemically possible for the ratio. This value indicates an overcorrection, or that R_{pON} is varying around the zero value

(small positive and negative) when the air mixture is strictly inorganic nitrate free. Thus, for calculation purposes, we use $R_{\text{pON}} = 0.0001$ to represent the smallest possible NO_x^+ ratio for CV-ACSM measurements.

As the *RoR* from the experiments (including Hu et al. (2017), $RoR = 13.3$) are very different, we set the upper limit of R_{pON} to be R_{pON} obtained using $RoR = 3.29$, and the lower limit to be $R_{\text{pON}} = 0.0001$ in CV. The calculated R_{pON} for two CV-ToF-ACSM deployed in this study are summarized in Table 2. These limits are used to determine the uncertainty of f_{pON} calculation. Since we see the tendency of m/z 46 signal intensity (and thus NO_2^+) to be produced in the vaporizer in relatively small quantities compared to NO^+ , the tendency of R_{pON} therefore is also to approach zero (non-normal distribution). With only limited information about R_{pON} in CV unlike SV, we use the geometric mean instead of arithmetic mean to establish the expected central value of R_{pON} . We note that it is common to use geometric means to estimate averages of ratios.

Table 2. Summary of measured R_{pAmN} (including uncertainties) and calculated R_{pON} (upper and lower limits as determined from pON in glyoxal+ NO_3 chamber experiment). The geometric mean is considered as central value since R_{pON} is likely approaching zero. Values are for ACSM-UU (employed for ambient measurements in Cabauw) and the ACSM-RUG (employed for AIDA chamber experiments).

Instrument Measurements	ACSM-UU Cabauw ambient air		ACSM-RUG chamber experiment	
	R_{pAmN}	R_{pON}	R_{pAmN}	R_{pON}
Upper limit		0.0072 ^(a)		0.0035 ^(b)
Geometric mean	0.0237 ± 0.0009	0.0008 ^(c)	0.0115 ± 0.0002	0.0006 ^(c)
Lower limit		0.0001 ^(d)		0.0001 ^(d)

^(a) Calculated using $RoR = 3.29$. The RoR is obtained using R_{pON} from the upper limit experiment of glyoxal+ NO_3 and measured R_{pAmN} , using ACSM-RUG (see Fig. 2).

^(b) Experimental NO_x^+ ratio value from the lower limit experiment of glyoxal+ NO_3 using ACSM-RUG (see Fig. 2a).

^(c) Geometric mean of the upper and lower limit R_{pON} .

^(d) Set as the lowest possible NO_x^+ ratio in CV-based instruments, approaching zero.

Since the R_{pAmN} values are quite different for the two ACSMs used in this study as we see in Table 2, the upper limit R_{pON} are also different by almost a factor of 2. However, since the lower limit of R_{pON} approaches zero, the geometric means of the upper and lower limits for the two instruments differ by only 25%. While calibrating every instrument with a pure organic nitrate aerosol standard would be a preferable way to establish R_{pON} , we recognize the unlikelihood of that for all monitoring ACSMs. Therefore, we recommend this *RoR*-based approach. As will be shown in the following section, despite the uncertainties outlined here based on potential impurities in our “pure pON” chamber experiment, the nitrate splitting performs encouragingly well, with both ACSMs.

5 Development of NO_x^+ ratio method for CV-UMR-ToF-ACSM

5.1 Challenges in NO_x^+ ratio method application to CV-UMR-ToF-ACSM dataset

Applying the NO_x^+ ratio method to separate pAmN and pON in CV-UMR-ToF-ACSM datasets is a greater challenge than with SV, due primarily to the higher detection limit of NO_3 . The detection limit of p NO_3 in CV-UMR-ToF-ACSM is 0.01-0.08 $\mu\text{g m}^{-3}$ (from this work and Zheng et al. (2020) converted), around 10-100 times higher compared to those in SV-cToF-AMS ($\sim 0.6 \text{ ng m}^{-3}$ from Drewnick et al. (2009)) and SV-HR-ToF-AMS (0.1-4.0 ng m^{-3} from DeCarlo et al. (2006)), all converted to 10 min time resolution.

The poor detection limit for NO_x^+ ratios in CV-ToF-ACSM results from the low signal for m/z 46 relative to m/z 30 that are used to calculate frag_ NO_3 [30] (C_{NO^+}) and frag_ NO_3 [46] ($C_{\text{NO}_2^+}$). For instance, using the ACSM-UU, the detection limit of NO_2^+ is comparable to the detection limit of NO^+ at p NO_3 concentration near the detection limit of p NO_3 ($C_{\text{DL,NO}_2^+} = 0.044 \mu\text{g m}^{-3}$; $C_{\text{DL,NO}^+} = 0.066 \mu\text{g m}^{-3}$; for $C_{\text{DL,pNO}_3} = 0.075 \mu\text{g m}^{-3}$; all in 10 min time resolution). However, the magnitude of observed NO_2^+ from ambient measurements is 25-500 times lower than NO^+ in CV-ToF-ACSM. This means the NO_2^+ signal intensity is regularly close to the detection limit, particularly when the total p NO_3 concentration is low. This behavior also leads to noisy R_{obs} , due to a computation of very low or negative NO_2^+ signals, poor baseline, or both.

5.2 Data pre-treatment: Time averaging and data filtering

To determine which data points are reliable for R_{obs} calculation in the dataset, we could discard observed NO_2^+ signal intensities that are below the detection limit. However, this would result in removing nearly all the data, including data that, while low and noisy, can still provide quantitative information with adequate averaging. Therefore, we use observed NO^+ signals as the filtering parameter. The NO^+ signal accounts for $\sim 95\%$ of the total concentration of NO_3 species measured by ToF-ACSM (no RIE applied) and thus is a good indicator of when both NO^+ and NO_2^+ signals are too uncertain.

Eq. 4 describes the NO^+ signal limit ($C_{\text{NO}^+, \text{lim}}$) which assures reliable separation of f_{pON} and f_{pAmN} calculated using the detection limit of NO_2^+ ($C_{\text{DL,NO}_2^+}$) and R_{pAmN} as filter NO_x^+ ratio. We choose the larger R_{pAmN} value, which is a less strict limit relative to R_{pON} value, but still keeps any data with sufficiently good signal-to-noise ratio. The measured data points with observed NO^+ signal intensity below these criteria are replaced with not-a-number (nan).

$$C_{\text{NO}^+, \text{lim}} = \frac{C_{\text{DL,NO}_2^+}}{R_{\text{pAmN}}} \quad (4)$$

On this basis, we recommend data pre-treatments by time averaging and data filtering using observed NO^+ signal contribution as parameter. Time averaging over longer time periods allows the reduction of the electronic noise coming from the instrument response and low counting statistics associated with sampling ambient air. Meanwhile, the data filtering serves to determine the minimum p NO_3 concentration at which reliable R_{obs} can be obtained to calculate f_{pON} and f_{pAmN} .

The values of $C_{\text{DL,NO}_2^+}$ and $C_{\text{NO}^+, \text{lim}}$ in different time averaging are evaluated in Table 3 for the CV-ToF-ACSM deployed for ambient measurements in Cabauw, the Netherlands. The signal limit is lower as the time resolution increases due to the

improvement of detection limit with better statistics. For measurements in this study, the minimum reliable C_{NO^+} for 10 min, 30 min, 60 min, and 120 min time resolution are 1.88, 1.08, 0.77, and $0.54 \mu\text{g m}^{-3}$, respectively.

335 With these $C_{\text{NO}^+, \text{lim}}$, we performed data filtering to the ambient measurement time series from Cabauw in different averaging of the time series. The time averaging (generated by Tofware v3.3) is applied first before the data filtering to maximize retained data in the concentration average.

Table 3. Detection limits of NO_2^+ and signal limits for NO^+ across different time averaging with R_{pAmN} as filter NO_x^+ ratio for the CV-UMR-ToF-ACSM deployed for ambient measurements in the rural site of Cabauw, the Netherlands (ACSM-UU).

Signal intensity ($\mu\text{g m}^{-3}$)	10 min	30 min	60 min	120 min
$C_{\text{DL}, \text{NO}_2^+}$	0.044	0.026	0.018	0.013
$C_{\text{NO}^+, \text{lim}}$ (filter: $R_{\text{pAmN}} = 0.0237$)	1.88	1.08	0.77	0.54

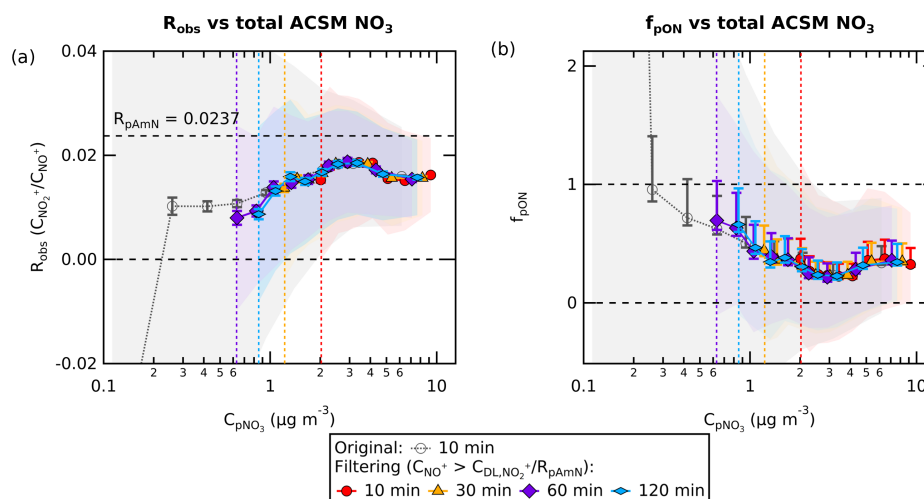


Figure 3. Chemical coordinate plots (a) between R_{obs} against C_{pNO_3} in Cabauw (net 205 days of data), and (b) between the f_{pON} calculated using geometric mean of R_{pON} ($R_{\text{pON}} = 0.0008$) against C_{pNO_3} . The revised fragmentation table for typical ambient dataset is used to obtain C_{NO^+} and $C_{\text{NO}_2^+}$. The line and marker traces represent the quantile average. The colored shading represents the standard deviation of each quantile while the whisker is the standard error. The standard deviation and standard error both include the uncertainty of ion counting statistics from measurements and uncertainty from ODR fit slope of fragmentation table correction. For f_{pON} (plot b), the standard deviation and standard error also include the uncertainty from lower and upper limit of R_{pON} ($R_{\text{pON}} = 0.0001$; $R_{\text{pON}} = 0.0072$). All analyses were done using the 10 min, 30 min, 60 min, and 120 min averaging of the time series, with data filtering. The original 10 min data without pre-treatment is also included as comparison. The combination of data filtering and time averaging reduces the noise compared to original data and improves the minimum concentration reliable for apportionment calculation (pNO_3 concentration limit for each time average, as indicated with vertical dashed lines).

Chemical coordinate plots of R_{obs} and f_{pON} against the total concentration of particulate nitrate (C_{pNO_3}) are shown in Fig. 3. These plots show the quantile average of the output variable on the y-axis (i.e. R_{obs} or f_{pON}) as a function of concentration bins in the x-axis (C_{pNO_3}). Fig. 3a,b shows that data filtering removes extreme R_{obs} and f_{pON} values near detection limit level. The fact that the chemical coordinate trends are consistent across different averaging times indicates that filtering to remove noisy data will not bias the interpretation of the ensemble dataset. The value of treating the data as a chemical coordinate plot is to allow for a robust characterization of the average trend, even using a method with substantial uncertainties. Importantly, the standard errors represent how well the averages are known. Their small uncertainty ranges support that the trend characterized is robust.

The combination of data filtering and time averaging shows different concentration cut-off for calculation of the NO_x^+ ratio. The concentration cut-off is lower for longer averaging times due to the improvement of $C_{\text{DL,NO}_2^+}$. For measurements in this study, the C_{pNO_3} cut-off for 10 min, 30 min, 60 min, and 120 min time averaging are 2.0, 1.2, 0.9, and $0.6 \mu\text{g m}^{-3}$, respectively. Because there is a trade-off between time resolution and the concentration cut-off, for a given dataset, the timescale of typical variations should be assessed in order to determine the appropriate averaging time.

5.3 Propagation of uncertainty

We propagated uncertainties from the variables in f_{pON} using simplified propagation of uncertainties using standard error (Day et al. (2023); see Section S4.3 of SI for details). The uncertainty of the final function (s_f) is calculated using the standard error (s_{x_i}) and partial derivative of the function ($\frac{\partial f}{\partial x_i}$) of each measurand (x_i) using Eq. 5.

$$s_{f(x_i, x_{i+1}, \dots)} = \sqrt{\sum_{i=1}^N \left(\frac{\partial f(x_i, x_{i+1}, \dots)}{\partial x_i} \right)^2 \cdot s_{x_i}^2} \quad (5)$$

The uncertainty of f_{pON} arises from three terms: R_{obs} , R_{pAmN} , and R_{pON} . For R_{obs} , the uncertainty is further composed of 6 components that make up NO^+ and NO_2^+ signals (the uncertainties of m/z 29, m/z 30, m/z 45, and m/z 46 related to precision uncertainty from electronic noise and ion counting statistics, and the uncertainties of the fragmentation table multipliers, represented by the uncertainty of ODR fit slope). For R_{pAmN} , we propagate the uncertainty of the mean NO_x^+ ratio from repeated NH_4NO_3 measurements using ODR fit to consider the instrument stability in acquiring the NO_x^+ ratio over time. For R_{pON} , the uncertainty is set to zero. Instead, the lower and upper limit of R_{pON} (see Table 2) serve to give a range of final propagated uncertainty, which includes R_{obs} , R_{pAmN} , and R_{pON} .

Fig. 4a shows that low pNO_3 concentrations produce larger uncertainties in f_{pON} ($s_{f_{\text{pON}}}$) compared to higher concentrations. If we compare the analysis with and without data filtering, we observe that filtering targets data points with high absolute $s_{f_{\text{pON}}}$ (above ± 0.5). We avoid removing many data points in the low concentration range by performing time averaging, where the average uncertainty decreases by $\sim \sqrt{N}$ for each N -fold of averaging from 10 min. Meanwhile, the uncertainties from R_{pAmN} and R_{pON} (RoR) remain unaffected by time averaging because the values remain constant in the time series.

Several studies reported f_{pON} lower than 20%, which occur mainly in urban areas and during a colder period. Yu et al. (2024) observed a lower range of annual average of urban f_{pON} in China to be $\sim 17\%$, while Mohr et al. (2012) and Pandolfi et al.

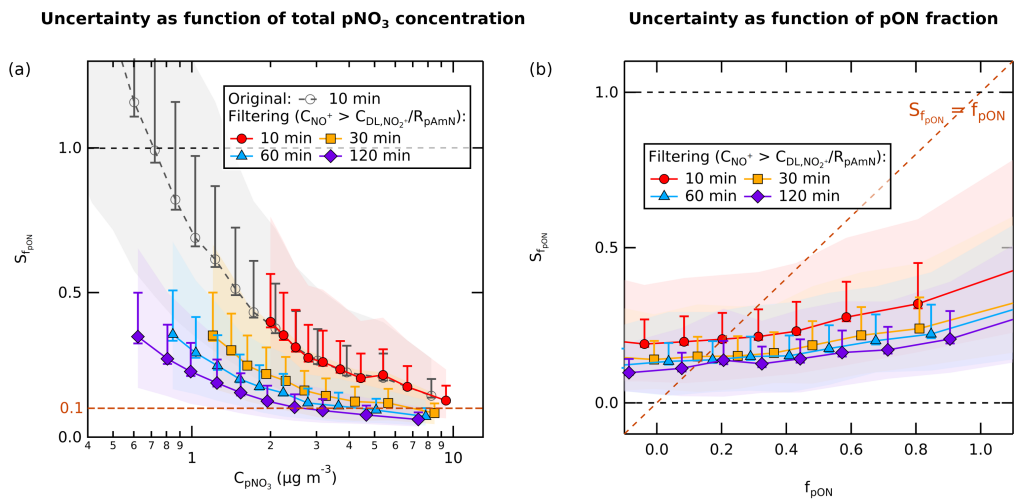


Figure 4. The chemical coordinate plot (quantile average) between (a) $s_{f_{\text{PON}}}$ and C_{pNO_3} (logarithmic scale), and (b) $s_{f_{\text{PON}}}$ and f_{PON} (linear scale), with $R_{\text{pAmN}} = 0.0237$ as filter NO_x^+ ratio at various averaging of the time series. The line and marker trace represents the average uncertainty produced from the geometric mean of f_{PON} . The uncertainty consists of uncertainties of ion counting statistics from measurements, uncertainty from ODR fit slope of fragmentation table correction, and uncertainty of R_{pAmN} . The colored shading represents the standard deviation of each quantile, while the whisker is the standard error. The shading and whisker both include the uncertainty of R_{pON} coming from the lower and upper limit of R_{pON} ($R_{\text{pON}} = 0.0001$ and $R_{\text{pON}} = 0.0072$), and also the uncertainty of the average quantile. Uncertainties of $f_{\text{PON}} < 0.1$ (absolute value) is reached at pNO₃ concentration $> 10 \mu\text{g m}^{-3}$ for 10 min time averaging, while at 60 min, it is reached already at $\sim 4 \mu\text{g m}^{-3}$. In terms of fraction, uncertainties of f_{PON} below the calculated f_{PON} ($s_{f_{\text{PON}}} < f_{\text{PON}}$) is reached at $f_{\text{PON}} \sim 0.2$ for 10 min averaging, while at 60 min, it is reached at $f_{\text{PON}} \sim 0.17$.

370 (2014) reported $\sim 13\%$ fraction in Barcelona, Spain, and Xu et al. (2021) reported 9.8% fraction in wintertime Beijing, China. If we use the lower range of f_{PON} of $\sim 10\%$ as reference for the minimum uncertainty needed to report reliable f_{PON} , we can observe that the lowest pNO₃ where we obtain below 0.1 absolute uncertainty in f_{PON} decreases along with time averaging as well. Uncertainties below ± 0.1 can only be reached at pNO₃ concentration higher than 10, 7, 4, 2 $\mu\text{g m}^{-3}$ at 10, 30, 60, and 120 min time averaging, respectively.

375 Fig. 4b shows the relationship between the absolute $s_{f_{\text{PON}}}$ and f_{PON} . The limit at which the absolute value of $s_{f_{\text{PON}}}$ is below or equal to f_{PON} (minimum uncertainty) is found to be 20%, 15%, 14%, 12% at 10, 30, 60, and 120 min time averaging, respectively. This result suggests that the NO_x^+ ratio method in CV-UMR-ToF-ACSM is more reliable to analyze nitrate pollution episodes or chamber experiments, and not for low background pNO₃ concentrations. By combining both the concentration limit and the fraction limit, we suggest that in the region where pNO₃ concentration is $< 10 \mu\text{g m}^{-3}$ and/or $f_{\text{PON}} < 12\%$, the
 380 method requires a longer time average to calculate f_{PON} to achieve minimum uncertainty.

6 Case studies demonstrating NO_x^+ ratio method for CV-ToF-ACSM

6.1 Ambient measurements at rural site

In order to demonstrate the efficacy of this method, we investigate the trend of f_{pON} and f_{pAmN} in the dataset observed at Cabauw. The ambient concentration time series of pAmN and pON (using $R_{\text{pAmN}} = 0.0237$ and $R_{\text{pON}} = 0.0008$) is compared
385 with the ACSM measured Org and NH4 fractions, shown in Fig. 5. The time series is averaged to 60 min and filtered using $R_{\text{pAmN}} = 0.0237$ (values of $C_{\text{NO}^+} < C_{\text{DL,NO}_2^+}/R_{\text{pAmN}}$ are discarded). We observe that f_{pON} increases with increasing fraction of organic aerosol concentration in total ACSM $\text{PM}_{2.5}$ ($C_{\text{OA}}/C_{\text{PM}_{2.5}}$, from 48% to 64%), whereas the f_{pAmN} increases with increasing fraction of particulate ammonium concentration in total ACSM $\text{PM}_{2.5}$ ($C_{\text{pNH}_4}/C_{\text{PM}_{2.5}}$, from 8% to 15%). This shows that the organic nitrate fraction is correlated with availability of organics (particularly at high organics fraction), while
390 the inorganic fraction increases with available NH_4 (particularly at low ammonium fraction).

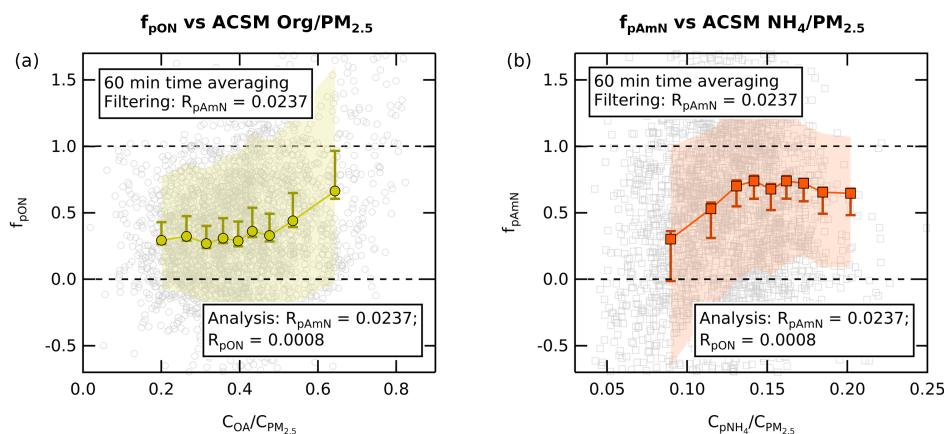


Figure 5. (a) The chemical coordinate plot (quantile average) of f_{pON} against $C_{\text{OA}}/C_{\text{PM}_{2.5}}$ shows an average increase of f_{pON} as OA fraction increases from 48% to 64%, where the f_{pON} varies from 33% to 66%. (b) The chemical coordinate plot (quantile average) of f_{pAmN} against $C_{\text{pNH}_4}/C_{\text{PM}_{2.5}}$ shows an average increase of f_{pAmN} as pNH₄ fraction increases from 8% to 15%, where the f_{pAmN} varies from 30% to 74%. Note: All quantile averages were calculated using the 60 min averaging of the time series. The colored shading is the standard deviation of each quantile average, while the whiskers represent the standard error. They include the uncertainties of ion counting statistics from measurements, uncertainty from ODR fit slope of fragmentation table correction, and R_{pON} range value.

We also investigate specific nitrate episodes to show the composition of pON and pAmN in ambient pollution events. The time series of the NO_x^+ ratios, ACSM species concentrations (OA, pNH₄, pNO₃), pAmN and pON concentrations are shown in Fig. 6. Four nitrate episodes from spring (15 May 2023), summer (23 June 2023), autumn (05-06 September 2023), and winter (11 January 2024) are shown. The uncertainty of the concentration is obtained by combining the uncertainty from the
395 nitrate fraction (f_{pON} or f_{pAmN}), the total ACSM NO_3 , and the R_{pON} value range (see Eqs. S14 and S15). Note that the reported uncertainties are only related to precision uncertainty, and not to concentration quantification (e.g., ionization efficiency) like

the one described by Bahreini et al. (2009) (see details in Section S4.3 of SI). We observe that the adapted NO_x^+ ratio method is able to separate contributions of pON and pAmN to the total p NO_3 concentration. In Fig. 6i,ii,iv, we can see that the time series of pON tracks with total OA, while pAmN tracks with p NH_4 in the rural site. In Fig. 6iii, no significant trend is observed for pON due to lower mass loading of p NO_3 .

Unless there are co-located ambient measurements of UMR and HR instruments, the reported concentration of NO_3 in pON depends on the value of R_{pON} and multipliers used to calculate NO^+ and NO_2^+ signal contribution in the fragmentation table. The sensitivity of these variables needs to be assessed to understand which parameter is the most critical in the separation of inorganic and organic nitrate signal from ACSM.

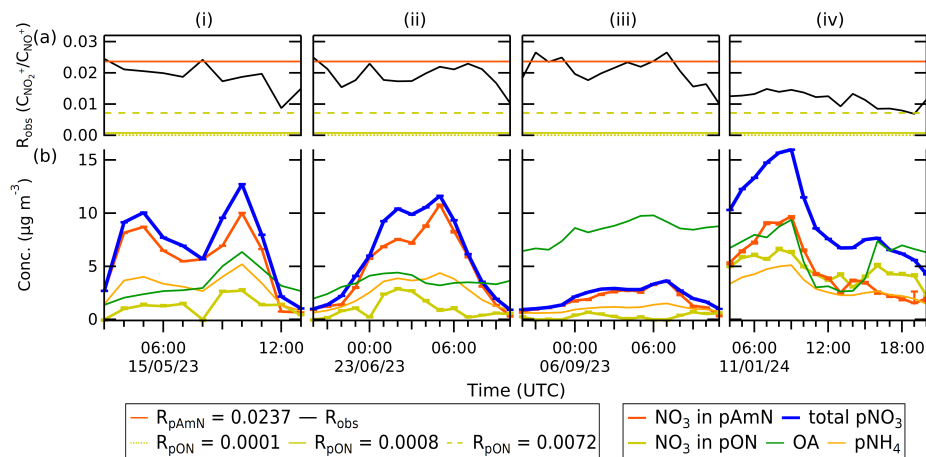


Figure 6. The time series for select periods of (a) R_{obs} , with horizontal lines indicating the values for R_{pAmN} and R_{pON} , (b) mass concentration of ACSM-measured total OA, p NH_4 , and p NO_3 , and pAmN and in pON. The separation of pAmN and pON is calculated using $R_{\text{pAmN}} = 0.0237$ and $R_{\text{pON}} = 0.0008$. The whiskers represent the uncertainty from nitrate fraction (f_{pON} or f_{pAmN}), precision uncertainty of total ACSM NO_3 from Tofware v3.3, and the R_{pON} value range. The time series (i), (ii), (iii), (iv) represents representative composition in spring, summer, autumn, and winter, all in 60 min time averaging.

In Fig. 7, we show the sensitivity analysis of R_{pON} , $a_{\text{Org}[30],[29]}$ and $a_{\text{Org}[46],[45]}$. We varied R_{pON} from zero to $R_{\text{pON}} = 0.0072$ (calculated using $RoR = 3.29$). Fig. 7a suggests that for $R_{\text{pON}} \leq 10^{-3}$, the reported pON concentrations are not significantly different and therefore confirm the lower limit of R_{pON} approaching zero, as established in Table 2. The value of R_{pON} calculated using RoR (in this case $R_{\text{pON}} = 0.0072$) shows relatively higher pON concentration, which is consistent with its use as the upper limit of R_{pON} .

We also varied $a_{\text{Org}[30],[29]}$ and $a_{\text{Org}[46],[45]}$ using the values listed in Table S4 and Fig. S1c,d in SI. Fig. 7b shows that the calculated pON concentration is sensitive to $a_{\text{Org}[46],[45]}$, which is not the case for $a_{\text{Org}[30],[29]}$. It further demonstrates that the limitation of this adapted NO_x^+ ratio method is its sensitivity towards $a_{\text{Org}[46],[45]}$ to obtain NO_2^+ signal contribution. Chemically, this suggests that the organic contribution in m/z 46 can vary and comprises a substantial portion of the total m/z 46 signal. Therefore, an average correction for m/z 46 may result in a high uncertainty of calculated f_{pON} using the NO_x^+ ratio method.

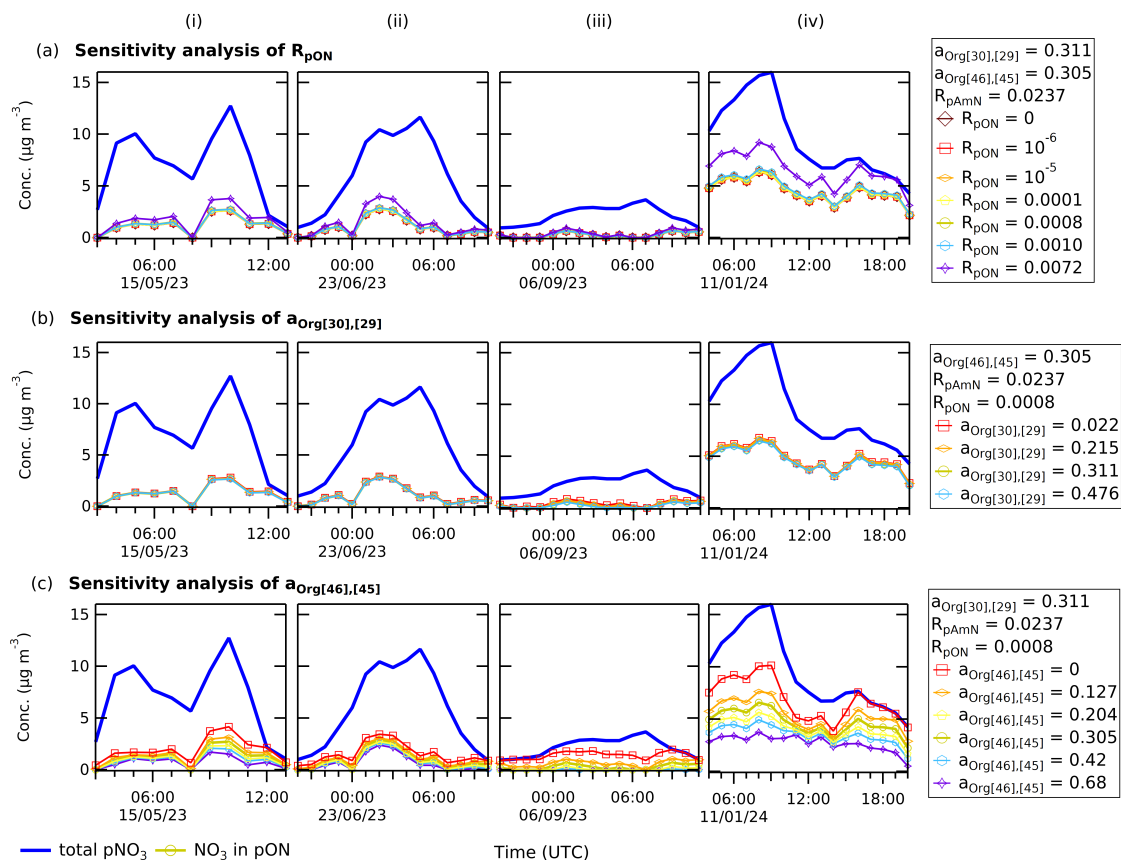


Figure 7. Sensitivity analysis of (a) R_{pON} , (b) $a_{\text{Org}[30],[29]}$, and (c) $a_{\text{Org}[46],[45]}$ to the pON concentration (NO_3 in pON) calculated using adapted NO_x^+ ratio method. The time series in each case is an ambient pollution episode in Cabauw, the Netherlands, during spring, summer, autumn, and winter period (i-iv). The results show that (a) $R_{\text{pON}} \leq 10^{-3}$ does not show significant differences in reported pON concentration, and (b) the reported pON concentration is not sensitive to the change of $a_{\text{Org}[30],[29]}$. In contrast, the results (c) show a significant change in reported pON concentration when $a_{\text{Org}[46],[45]}$ is varied, showing that this correction is the primary limitation of the NO_x^+ ratio method in CV-ACSM, because it can be highly dependent on the calculation of NO_2^+ signal contributions to m/z 46.

415 This was considered in the propagation of uncertainty, where we take into account the changing $a_{\text{Org}[46],[45]}$ in the reported f_{pON} , therefore representing a range of the observed organic nitrate contribution.

6.2 pAmN and pON formation in chamber experiment

We investigated the pAmN and pON formation in a chamber experiment using limonene precursor, NO_3 oxidant, and with AmN seed aerosol. The experiment was carried out in the AIDA chamber. Alongside CV-UMR-ToF-ACSM (ACSM-RUG), a
 420 SV-HR-ToF-AMS managed by IMK KIT was also deployed.

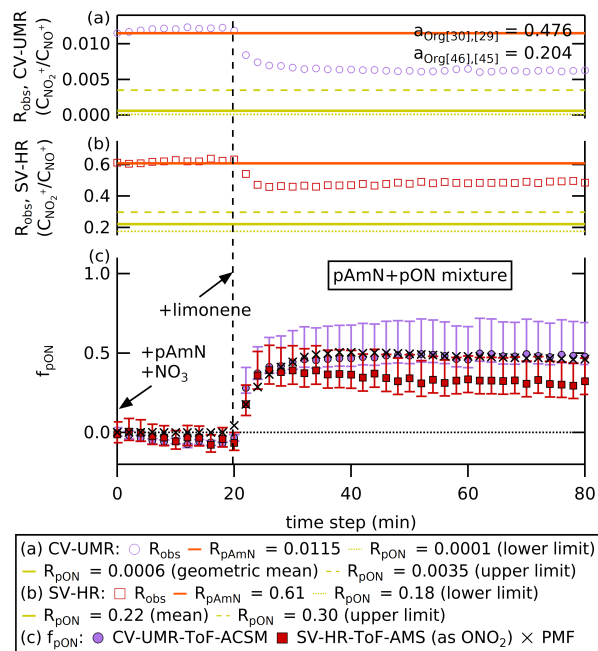


Figure 8. (a,b) The time series in 2 min time averaging of R_{obs} , R_{pAmN} , and R_{pON} measured by CV-UMR-ToF-ACSM (top) and SV-HR-ToF-AMS (middle). The fragmentation table specific for terpene is used to obtain the $C_{\text{NO}_x^+}$ and $C_{\text{NO}_2^+}$ of the chamber experiment. (c) The time series in 2 min time averaging of f_{pON} from NO_x^+ ratio method applied to SV-HR-ToF-AMS and CV-UMR-ToF-ACSM, as well as PMF method applied to CV-UMR-ToF-ACSM. The markers represent geometric mean for NO_x^+ ratio method applied to CV-UMR-ToF-ACSM (circle), mean for NO_x^+ ratio method of SV-HR-ToF-AMS (square) and for PMF method of CV-UMR-ToF-ACSM (cross). The whiskers represent the uncertainties from the value range of R_{pON} combined with the uncertainties from electronic noise, ion counting statistics, fragmentation table (for UMR), and R_{pAmN} . The uncertainty from the PMF analysis is not shown for simplicity.

The ACSM data is analyzed using the revised fragmentation table specific for terpene chamber experiments (see Section 3.2), while the AMS data is analyzed using Squirrel 1.66E and PIKA 1.26E with the default ion list. Although the time resolution is 2 min, time averaging and data filtering is not necessary since the experiment involves high concentrations. The lower limit, geometric mean, and upper limit of R_{pON} ($R_{\text{pON}} = 0.0001$; 0.0006 ; 0.0035 , respectively) are employed to estimate the uncertainty of f_{pON} , alongside $R_{\text{pAmN}} = 0.0115$ (see Table 2). For the AMS instrument, the measurements of pure pAmN give $R_{\text{pAmN}} = 0.61 \pm 0.05$ and the R_{pON} value is calculated using $R_{\text{O}R} = 2.75 \pm 0.70$ (Day et al., 2022a), which gives $R_{\text{pON}} = 0.18$; 0.22 ; 0.30 as lower limit, mean, and upper limit, respectively.

We also performed PMF analysis using the ACSM data including OA, NO_x^+ , and NH_x^+ ions, which has been similarly done in other studies (e.g., Day et al. (2022a) and references therein). The 2 min average matrices of UMR organic fragment mass spectra with a m/z of 12 to 120, fragments of ammonium ($\text{NH}_4\text{-16}$ and $\text{NH}_4\text{-17}$, two main signals of NH_4 which are NH_2^+ and NH_3^+), and fragments of nitrate ($\text{NO}_3\text{-30}$ and $\text{NO}_3\text{-46}$, two main signals of NO_3 which are NO^+ , NO_2^+) are used as

variables in the PMF input matrix. Fragment contributions are calculated using the terpene-related fragmentation table (see Section 3.2). We choose a two-factor solution (see Fig. S2) because we are interested in splitting the aerosol mass only into inorganic aerosol (pAmN) and organic aerosol (OA mixture, containing pON). From the organic aerosol factor, we calculate
435 the f_{pON} from the factor concentration time series. The details of the PMF method are described in Section S5, including the statistical summary and the diagnostic plots of the PMF analysis.

The NO_x^+ ratio and f_{pON} time series for the limonene SOA experiment are shown in Fig. 8. The whiskers around the mean f_{pON} represents the uncertainties coming from the value range of R_{pON} combined with the uncertainties from ion counting statistics, electronic noise, fragmentation table (for UMR), and R_{pAmN} (see Section 5.3). The initial mixture of NH_4NO_3 seed
440 and NO_3 radical from NO_2 and O_3 gives a ratio that matches R_{pAmN} from an offline calibration, where f_{pON} is close to zero for both instruments. Although nitric acid (HNO_3) can be formed by nitrogen pentoxide (N_2O_5) hydrolysis under these humid conditions, experiments were run in excess NH_3 and therefore we expect no substantial increase of HNO_3 that can affect NO_x^+ ratio. After the limonene injection, the R_{obs} rose to values in between R_{pAmN} and R_{pON} , indicating the formation of a mixture of pAmN and pON inside the chamber.

445 Based on observations of Takeuchi et al. (2024), pON measured with the SV-AMS is only quantitatively detected as $-\text{NO}_2$ moiety, not $-\text{ONO}_2$. The reasoning for this difference in detection of alkyl nitrate (RONO_2) and NH_4NO_3 is thought to be due to thermal decomposition of pON producing NO_2 gas in the vaporizer, while NH_4NO_3 would more likely decompose to HNO_3 , and thus dominantly ionizing gases of different molecular weights. The “missing oxygen” is generally retained bound to the carbon, and thus accounted as organic moiety. Thus, f_{pON} needs to be corrected for this phenomenon using molar mass
450 ratio of NO_3/NO_2 ($62 \text{ g mol}^{-1}/46 \text{ g mol}^{-1}$) to recalculate the pON mass. There is no study yet assessing the necessity of correcting f_{pON} in CV, and we suggest that it is likely unnecessary due to the more complete thermal decomposition that shifts the fragmentation pattern of both NH_4NO_3 and RONO_2 to NO_2 and NO .

Both NO_x^+ ratio methods (SV-AMS and CV-ACSM) and the PMF method (CV-ACSM) show a similar response to the injection of limonene, whereupon f_{pON} increases rapidly from ~ 0 to 0.3-0.5. The agreement between the two instruments on
455 this initial pON production is encouraging. However, after this initial jump, the trend of f_{pON} seems to vary. While mean f_{pON} calculated using NO_x^+ ratio method from CV-ACSM remains steady after the injection, the other two results show a gradual decrease of f_{pON} as the chamber dilutes.

The NO_x^+ ratio method on CV-ACSM data shows a similar change in f_{pON} relative to the PMF method immediately after limonene injection but then continues to decrease over time (see Fig. 8). The PMF method combines the variations of Org,
460 NO_x^+ , and NH_x^+ ions to obtain the factor profiles, therefore allowing a more subtle change in the chamber composition to be taken account. The NO_x^+ ratio method in CV-UMR, in contrast, only takes into account fragments that are in m/z 30 and m/z 46 using constant fragmentation table relationship.

Similarly, the SV-AMS also shows a gradual decrease of mean f_{pON} unlike the NO_x^+ ratio method from CV-ACSM (see Fig. 8). This suggests that changing contributions of organics at m/z 30 and m/z 46 may be taken into account by HR peak fitting
465 and not by the UMR fragmentation table, causing a divergence as the chamber aerosol dilutes. Based on the sensitivity analysis in Fig. 7, the signal contribution of NO_2^+ (m/z 46) is the largest source of uncertainty in the CV-ACSM, since the adapted

method is sensitive to the change of $a_{\text{Org}[46],[45]}$. On the other hand, the uncertainty of R_{OR} used to calculate R_{pON} accounts for the largest contribution to the uncertainty calculated for SV-AMS. Since the R_{OR} in Day et al. (2022a) relies on the average value of a broad range of organic nitrate, a chamber experiment that uses a specific precursor is likely to have R_{pON} further away from the average value than, for instance, a complex ambient mixture.

Nevertheless, we are encouraged by the match in responses upon formation of organic nitrate, indicating that the NO_x^+ ratio method is similarly sensitive to changing nitrate speciation in both instruments. When considering the propagation of uncertainty, we observe overlaps between the results of CV-ACSM and SV-AMS. Therefore, by considering the uncertainty from $a_{\text{Org}[46],[45]}$ in CV-UMR and uncertainty from R_{OR} in SV-AMS, the results for both instruments are comparable. Further investigation of the detailed response of each instrument to changing aerosol composition would be valuable.

7 Conclusions and recommendations

We have shown the separation of particulate ammonium nitrate (pAmN) and particulate organic nitrate (pON) signal from total particulate nitrate (pNO_3) signal measured using time-of-flight aerosol chemical speciation monitor equipped with capture vaporizer in unit mass resolution (CV-UMR-ToF-ACSM), using an adapted NO_x^+ ratio method with a revised fragmentation table and data pre-treatment. The shift of fragmentation pattern towards smaller ion fragments in the capture vaporizer (CV) compared to the standard vaporizer (SV) affects the signals of NO^+ and NO_2^+ fragments and interferences by Org fragments used to calculate the NO_x^+ ratio in UMR. Therefore, we recommend updating the default fragmentation table from Allan et al. (2004) for entries shown in Table 4 before applying the NO_x^+ ratio method, according to the aerosol composition. As noted previously, substantial corrections to the fragmentation table for these terms have been shown to be needed for measurements using the SV under some conditions (Fry et al., 2018).

Table 4. Proposed m/z 30 and 46 entries for Org and NO_3 in the revised fragmentation table adapted for NO_x^+ ratio method in CV-UMR-ToF-ACSM. The multipliers ($a_{\text{Org}[x],[z]}$) are applied according to the aerosol composition. The entries that are not included in this table should follow the fragmentation table of Allan et al. (2004) for AMS and adapted without gas-phase corrections (frag_air) for ACSM.

m/z	Revised fragmentation table for CV-UMR-ToF-ACSM		$a_{\text{Org}[x],[z]}$			
	Org	NO_3	General	Biogenic ^(a)	Glyoxal	Terpene
30	$a_{\text{Org}[30],[29]} * \text{frag_Org}[29]$	[30], -frag_Org[30]	0.311	0.32	0.291	0.476
46	$a_{\text{Org}[46],[45]} * \text{frag_Org}[45]$	[46], -frag_Org[46]	0.305	0.68	0.082	0.204

^(a)Retrieved from Hu et al. (2017).

The shift of fragmentation pattern in the CV towards more formation of NO^+ fragments and less of NO_2^+ fragments changes the magnitude of the NO_x^+ ratio for both pure pAmN and pure pON. The NO_x^+ ratio in CV is affected by the aerodynamic lens alignment, and therefore we recommend users to align their aerodynamic lens to obtain the correct NO_x^+ ratio.

To separate the pAmN and pON signal from total pNO_3 and calculate the particulate organic nitrate fraction (f_{pON}), the regular ammonium nitrate calibration should be used to obtain the NO_x^+ ratio for pure ammonium nitrate (R_{pAmN}), where a

value of 0.01-0.07 is expected. On the other hand, we observed from a chamber experiment that the R_{pON} value approaches zero in the CV. Therefore, we recommend analyzing using three R_{pON} values, to describe the upper limit (R_{pON} calculated using $RoR = 3.29$), geometric mean, and lower limit ($R_{\text{pON}} = 0.0001$), which also provides f_{pON} uncertainty. If possible, we recommend constraining the RoR for more accurate results (e.g., performing chamber experiment to form pure organic nitrate). Through this study, we hope to inspire more research regarding R_{pON} measurement in CV-based instruments to obtain more precision in analyzing organic nitrate concentrations.

The observed NO_x^+ ratio (R_{obs}) tends to have more noise in CV-based measurements compared to SV. Data filtering using the instrument's R_{pAmN} and NO_2^+ detection limit has shown that the adapted NO_x^+ ratio method in the CV-UMR-ToF-ACSM is able to filter unreliable measurements with concentration cut-off ranging from 0.6 to 2.0 $\mu\text{g m}^{-3}$, depending on time averaging. This data pre-treatment filters data points with high fraction uncertainty (above ± 0.5) and decreases the average uncertainty by \sqrt{N} for each N -fold of averaging from 10 min.

With a longer time averaging, the concentration limit and fraction limit improve, which allows more reliable determination of f_{pON} and f_{pAmN} . The method reports absolute uncertainty of particulate organic nitrate <10% at the total particulate nitrate concentrations of 2 $\mu\text{g m}^{-3}$ (120 min time averaging) to 10 $\mu\text{g m}^{-3}$ (10 min time averaging) and organic nitrate fraction of 10% (120 min time averaging) to 20% (10 min time averaging). We recommend users to average the time series to 30 min or 60 min to retain information about real ambient variation, while improving the reliable nitrate concentration limit. This may also be convenient when comparing to auxiliary data that are typically reported half-hourly or hourly. In the region where pNO_3 concentration is <10 $\mu\text{g m}^{-3}$ and/or $f_{\text{pON}} < 12\%$, longer time averaging may be necessary to achieve the absolute uncertainty <10%. In studies where noise is not a problem (e.g., chamber experiments with high particle concentration), time averaging may be unnecessary. With a similar approach, this method could be used for SV-UMR-ToF-ACSM observations as well, with a fragmentation table suited for SV-based measurements.

The adapted NO_x^+ ratio method on rural nitrate episodes can distinguish periods with pAmN or pON as the major component, confirmed by relation to the ammonium and organic aerosol composition, respectively. The adapted NO_x^+ ratio method applied to CV-UMR-ToF-ACSM measurements in a chamber experiment is able to replicate the response to precursor injection observed from PMF analysis of the same measurements, as well as a co-located high-resolution time-of-flight aerosol mass spectrometer equipped with standard vaporizer (SV-HR-ToF-AMS). The largest uncertainties in this comparison come from $\alpha_{\text{Org}[46],[45]}$ (CV-UMR-ToF-ACSM) and RoR (SV-HR-ToF-AMS). The adapted NO_x^+ ratio method for CV-UMR-ToF-ACSM demonstrated in this study can be used at monitoring sites to monitor regional f_{pON} and improve understanding of particulate nitrate sources and evolution.

520 **Appendix A: List of terms and abbreviations**

Table A1: List of important terms and abbreviations used in the manuscript.

Terms	Name
ACSM	Aerosol Chemical Speciation Monitor
ACTRIS	Aerosol, Clouds and Trace Gases Research Infrastructure
AIDA	Aerosol Interaction and Dynamics in the Atmosphere
AmN	ammonium nitrate
AMS	Aerosol Mass Spectrometer
AmS	ammonium sulfate
$a_{\text{Org}[x],[i]}$	multiplier for calculating $\text{frag_Org}[x]$ based on the relationship between $\text{frag_Org}[x]$ and $\text{frag_Org}[i]$
C_ν	concentration/signal of species ν
$C_{\text{DL,NO}^+}$	detection limit of NO^+
$C_{\text{DL,NO}_2^+}$	detection limit of NO_2^+
$C_{\text{DL,pNO}_3}$	detection limit of pNO_3
C_{NO^+}	signal of NO^+
$C_{\text{NO}^+,\text{lim}}$	signal limit of NO^+ for reliable organic nitrate and ammonium nitrate separation
$C_{\text{NO}_2^+}$	signal of NO_2^+
C_{OA}	concentration of total organic aerosol
$C_{\text{PM}_{2.5}}$	concentration of total $\text{PM}_{2.5}$
C_{pNH_4}	concentration of total particulate ammonium
C_{pNO_3}	concentration of total particulate nitrate
CAINA	Cloud-Aerosol Interactions in a Nitrogen-dominated Atmosphere
CE	collection efficiency
Chl	chloride species in AMS/ACSM
cToF	compact time-of-flight
CV	capture vaporizer
f_{pAmN}	fraction of particulate ammonium nitrate to the total nitrate
f_{pON}	fraction of particulate organic nitrate to the total nitrate
$\text{frag_NO}_3[x]$	total nitrate fragments in nominal m/z x
$\text{frag_Org}[x]$	total organic fragments in nominal m/z x
HR	high resolution
IE	ionization efficiency
IMK	Institute for Meteorology and Climate Research
IPL	intermediate pressure lens

Continues next page

KIT	Karlsruhe Institute of Technology
KNMI	Royal Netherlands Meteorological Institute
m/z	mass-to-charge ratio
n	number of data
NO_x^+ ratio	NO_2^+ -to- NO^+ signal ratio
obs	observed data (ambient or chamber)
OA	organic aerosol
ODR	orthogonal distance regression
ON	organic nitrate
Org	total organic aerosol in AMS/ACSM
pAmN	particulate ammonium nitrate
PIKA	Peak Integration by Key Analysis
$\text{PM}_{2.5}$	particulate matter with size $<2.5\mu\text{m}$
PMF	Positive Matrix Factorization
pNH_4	particulate ammonium
pNO_3	particulate nitrate
pON	particulate organic nitrate
Q-ACSM	quadrupole-ACSM
R_ν	NO_x^+ ratio of ν
R_{obs}	NO_x^+ ratio of observed data
R_{pAmN}	NO_x^+ ratio of particulate ammonium nitrate
R_{pON}	NO_x^+ ratio of particulate organic nitrate
r^2	coefficient of determination
RIE	relative ionization efficiency
RONO_2	alkyl nitrate
R_oR	ratio-of-ratios
RUG	University of Groningen
s_f	uncertainty of function f
$s_{f_{\text{pON}}}$	uncertainty of particulate organic nitrate fraction to the total nitrate
s_{x_i}	standard error
SI	Supplementary Information
SOA	secondary organic aerosol
Squirrel	Sequential Igor Data Retrieval

Continues next page

SV	standard vaporizer
ToF	time-of-flight
UMR	unit mass resolution
UU	Utrecht University
VOCs	volatile organic compounds
WRF-Chem	Weather Research and Forecasting model coupled with Chemistry
x_i	measurand or measured value
$\frac{\delta f}{\delta x_i}$	partial derivative of the function f

Data availability. The CV-HR-ToF spectra used to build the revised fragmentation table are retrieved from the open access AMS spectral database (http://cires1.colorado.edu/jimenez-group/AMSsd_CV, last access: 6 November 2024). The CV-UMR-ToF-ACSM dataset were collected as part of the Ruisdael Observatory network monitoring (<https://ruisdael-observatory.nl>, last access: 6 November 2024) and are available upon request. The chamber experiment measurements using SV-HR-ToF-AMS and CV-UMR-ToF-ACSM (ACSM-RUG) were collected as part of the Cloud-Aerosol Interactions in a Nitrogen-dominated Atmosphere (CAINA) project (<https://sites.google.com/view/cainaproject/>, last access: 6 November 2024) in the Aerosol Interaction and Dynamics in the Atmosphere (AIDA) chamber managed by the Institute of Meteorology and Climate Research (IMK) in Karlsruhe Institute of Technology (KIT), Germany.

Author contributions. F.R.N.: conceptualization, investigation, writing, and editing. J.L.F. and D.A.D.: conceptualization, editing, and reviewing. R.M., R.H., S.H., J.F., J.M., and U.D.: resources, reviewing, and editing.

530 *Competing interests.* The contact author has declared that none of the authors has any competing interests.

Acknowledgements. This work has been accomplished by using data generated in the Ruisdael Observatory as part of continuous monitoring and the Cloud-Aerosol Interactions in a Nitrogen-dominated Atmosphere (CAINA) project. The Ruisdael Observatory is a scientific infrastructure co-financed by the Dutch Research Council (NWO; grant number 184.034.015). The CAINA project is a research consortium supported by NWO (grant number OCENW.XL21.XL21.112). D.A.D. was supported by NASA grant 80NSSC21K1451 and NSF grant AGS-2131914. The authors acknowledge valuable discussions and technical help with Anandi Williams, Phil Croteau, Donna Sueper, Weiwei Hu, Yanxia Li, Jean-Eudes Petit, Olivier Favez, Evelyn Freney, Hasna Chebaicheb, and Laurent Meunier.

References

- Adams, P. J., Seinfeld, J. H., and Koch, D. M.: Global concentrations of tropospheric sulfate, nitrate, and ammonium aerosol simulated in a general circulation model, *Journal of Geophysical Research: Atmospheres*, 104, 13 791–13 823, <https://doi.org/10.1029/1999JD900083>, 1999.
- 540 Allan, J. D., Delia, A. E., Coe, H., Bower, K. N., Alfarra, M., Jimenez, J. L., Middlebrook, A. M., Drewnick, F., Onasch, T. B., Canagaratna, M. R., Jayne, J. T., and Worsnop, D. R.: A generalised method for the extraction of chemically resolved mass spectra from Aerodyne aerosol mass spectrometer data, *Journal of Aerosol Science*, 35, 909–922, <https://doi.org/10.1016/j.jaerosci.2004.02.007>, 2004.
- Bahreini, R., Ervens, B., Middlebrook, A. M., Warneke, C., De Gouw, J. A., DeCarlo, P. F., Jimenez, J. L., Brock, C. A., Neuman, J. A., Ryerson, T. B., Stark, H., Atlas, E., Brioude, J., Fried, A., Holloway, J. S., Peischl, J., Richter, D., Walega, J., Weibring, P., Wollny, A. G., and Fehsenfeld, F. C.: Organic aerosol formation in urban and industrial plumes near Houston and Dallas, Texas, *Journal of Geophysical Research: Atmospheres*, 114, 2008JD011 493, <https://doi.org/10.1029/2008JD011493>, 2009.
- 545 Bauer, S. E., Koch, D., Unger, N., Metzger, S. M., Shindell, D. T., and Streets, D. G.: Nitrate aerosols today and in 2030: a global simulation including aerosols and tropospheric ozone, *Atmospheric Chemistry and Physics*, 7, 5043–5059, <https://doi.org/10.5194/acp-7-5043-2007>, 2007.
- 550 Bian, H., Chin, M., Hauglustaine, D. A., Schulz, M., Myhre, G., Bauer, S. E., Lund, M. T., Karydis, V. A., Kucsera, T. L., Pan, X., Pozzer, A., Skeie, R. B., Steenrod, S. D., Sudo, K., Tsigaridis, K., Tsimpidi, A. P., and Tsyro, S. G.: Investigation of global particulate nitrate from the AeroCom phase III experiment, *Atmospheric Chemistry and Physics*, 17, 12 911–12 940, <https://doi.org/10.5194/acp-17-12911-2017>, 2017.
- 555 Bobbink, R. and Hicks, W. K.: Factors Affecting Nitrogen Deposition Impacts on Biodiversity: An Overview, in: *Nitrogen Deposition, Critical Loads and Biodiversity*, edited by Sutton, M. A., Mason, K. E., Sheppard, L. J., Sverdrup, H., Haeuber, R., and Hicks, W. K., pp. 127–138, Springer Netherlands, Dordrecht, ISBN 978-94-007-7938-9 978-94-007-7939-6, https://doi.org/10.1007/978-94-007-7939-6_14, 2014.
- Brownwood, B., Turdziladze, A., Hohaus, T., Wu, R., Mentel, T. F., Carlsson, P. T. M., Tsiligiannis, E., Hallquist, M., Andres, S., Hantschke, L., Reimer, D., Rohrer, F., Tillmann, R., Winter, B., Liebmann, J., Brown, S. S., Kiendler-Scharr, A., Novelli, A., Fuchs, H., and Fry, J. L.: Gas-Particle Partitioning and SOA Yields of Organonitrate Products from NO₃-Initiated Oxidation of Isoprene under Varied Chemical Regimes, *ACS Earth and Space Chemistry*, 5, 785–800, <https://doi.org/10.1021/acsearthspacechem.0c00311>, 2021.
- 560 Canagaratna, M., Jayne, J., Jimenez, J., Allan, J., Alfarra, M., Zhang, Q., Onasch, T., Drewnick, F., Coe, H., Middlebrook, A., Delia, A., Williams, L., Trimborn, A., Northway, M., DeCarlo, P., Kolb, C., Davidovits, P., and Worsnop, D.: Chemical and microphysical characterization of ambient aerosols with the aerodyne aerosol mass spectrometer, *Mass Spectrometry Reviews*, 26, 185–222, <https://doi.org/10.1002/mas.20115>, 2007.
- 565 Carlton, A. G., De Gouw, J., Jimenez, J. L., Ambrose, J. L., Attwood, A. R., Brown, S., Baker, K. R., Brock, C., Cohen, R. C., Edgerton, S., Farkas, C. M., Farmer, D., Goldstein, A. H., Gratz, L., Guenther, A., Hunt, S., Jaeglé, L., Jaffe, D. A., Mak, J., McClure, C., Nenes, A., Nguyen, T. K., Pierce, J. R., De Sa, S., Selin, N. E., Shah, V., Shaw, S., Shepson, P. B., Song, S., Stutz, J., Surratt, J. D., Turpin, B. J., Warneke, C., Washenfelder, R. A., Wennberg, P. O., and Zhou, X.: Synthesis of the Southeast Atmosphere Studies: Investigating Fundamental Atmospheric Chemistry Questions, *Bulletin of the American Meteorological Society*, 99, 547–567, <https://doi.org/10.1175/BAMS-D-16-0048.1>, 2018.
- 570

- Day, D. A., Wooldridge, P. J., Dillon, M. B., Thornton, J. A., and Cohen, R. C.: A thermal dissociation laser-induced fluorescence instrument for in situ detection of NO₂, peroxy nitrates, alkyl nitrates, and HNO₃, *Journal of Geophysical Research: Atmospheres*, 107, 575 <https://doi.org/10.1029/2001JD000779>, 2002.
- Day, D. A., Campuzano-Jost, P., Nault, B. A., Palm, B. B., Hu, W., Guo, H., Wooldridge, P. J., Cohen, R. C., Docherty, K. S., Huffman, J. A., de Sá, S. S., Martin, S. T., and Jimenez, J. L.: A systematic re-evaluation of methods for quantification of bulk particle-phase organic nitrates using real-time aerosol mass spectrometry, *Atmospheric Measurement Techniques*, 15, 459–483, <https://doi.org/10.5194/amt-15-459-2022>, 2022a.
- 580 Day, D. A., Fry, J. L., Kang, H. G., Krechmer, J. E., Ayres, B. R., Keehan, N. I., Thompson, S. L., Hu, W., Campuzano-Jost, P., Schroder, J. C., Stark, H., DeVault, M. P., Ziemann, P. J., Zarzana, K. J., Wild, R. J., Dubè, W. P., Brown, S. S., and Jimenez, J. L.: Secondary Organic Aerosol Mass Yields from NO₃ Oxidation of α -Pinene and Δ -Carene: Effect of RO₂ Radical Fate, *The Journal of Physical Chemistry A*, 126, 7309–7330, <https://doi.org/10.1021/acs.jpca.2c04419>, 2022b.
- Day, D. A., Nault, B. A., Campuzano-Jost, P., and Jimenez, J. L.: Evaluation of Uncertainties and Introduction of Tools for Quantification 585 of Bulk Particle-phase Organic Nitrates Using Real-time Aerosol Mass Spectrometry, Portland, Oregon, https://aaarabstracts.com/2023/view_abstract.php?pid=88, 2023.
- DeCarlo, P. F., Kimmel, J. R., Trimborn, A., Northway, M. J., Jayne, J. T., Aiken, A. C., Gonin, M., Fuhrer, K., Horvath, T., Docherty, K. S., Worsnop, D. R., and Jimenez, J. L.: Field-Deployable, High-Resolution, Time-of-Flight Aerosol Mass Spectrometer, *Analytical Chemistry*, 78, 8281–8289, <https://doi.org/10.1021/ac061249n>, 2006.
- 590 Drewnick, F., Hings, S. S., DeCarlo, P., Jayne, J. T., Gonin, M., Fuhrer, K., Weimer, S., Jimenez, J. L., Demerjian, K. L., Borrmann, S., and Worsnop, D. R.: A New Time-of-Flight Aerosol Mass Spectrometer (TOF-AMS)—Instrument Description and First Field Deployment, *Aerosol Science and Technology*, 39, 637–658, <https://doi.org/10.1080/02786820500182040>, 2005.
- Drewnick, F., Hings, S. S., Alfarra, M. R., Prevot, A. S. H., and Borrmann, S.: Aerosol quantification with the Aerodyne Aerosol Mass Spectrometer: detection limits and ionizer background effects, *Atmospheric Measurement Techniques*, 2, 33–46, <https://doi.org/10.5194/amt-595-2-33-2009>, 2009.
- Drewnick, F., Diesch, J.-M., Faber, P., and Borrmann, S.: Aerosol mass spectrometry: particle–vaporizer interactions and their consequences for the measurements, *Atmospheric Measurement Techniques*, 8, 3811–3830, <https://doi.org/10.5194/amt-8-3811-2015>, 2015.
- Drugé, T., Nabat, P., Mallet, M., and Somot, S.: Model simulation of ammonium and nitrate aerosols distribution in the Euro-Mediterranean region and their radiative and climatic effects over 1979–2016, *Atmospheric Chemistry and Physics*, 19, 3707–3731, 600 <https://doi.org/10.5194/acp-19-3707-2019>, 2019.
- Erisman, J. W., Dammers, E., Damme, V., and Soudzilovskaia, N.: Trends in EU nitrogen deposition and impacts on ecosystems, p. 6, 2015.
- Farmer, D. K., Matsunaga, A., Docherty, K. S., Surratt, J. D., Seinfeld, J. H., Ziemann, P. J., and Jimenez, J. L.: Response of an aerosol mass spectrometer to organonitrates and organosulfates and implications for atmospheric chemistry, *Proceedings of the National Academy of Sciences*, 107, 6670–6675, <https://doi.org/10.1073/pnas.0912340107>, 2010.
- 605 Feng, Y. and Penner, J. E.: Global modeling of nitrate and ammonium: Interaction of aerosols and tropospheric chemistry, *Journal of Geophysical Research: Atmospheres*, 112, 2005JD006404, <https://doi.org/10.1029/2005JD006404>, 2007.
- Fields, S.: Global Nitrogen: Cycling out of Control, *Environmental Health Perspectives*, 112, <https://doi.org/10.1289/ehp.112-a556>, 2004.
- Fisher, J. A., Jacob, D. J., Travis, K. R., Kim, P. S., Marais, E. A., Chan Miller, C., Yu, K., Zhu, L., Yantosca, R. M., Sulprizio, M. P., Mao, J., Wennberg, P. O., Crounse, J. D., Teng, A. P., Nguyen, T. B., St. Clair, J. M., Cohen, R. C., Romer, P., Nault, B. A., Wooldridge, P. J., 610 Jimenez, J. L., Campuzano-Jost, P., Day, D. A., Hu, W., Shepson, P. B., Xiong, F., Blake, D. R., Goldstein, A. H., Misztal, P. K., Hanisco,

- T. F., Wolfe, G. M., Ryerson, T. B., Wisthaler, A., and Mikoviny, T.: Organic nitrate chemistry and its implications for nitrogen budgets in an isoprene- and monoterpene-rich atmosphere: constraints from aircraft (SEAC⁴RS) and ground-based (SOAS) observations in the Southeast US, *Atmospheric Chemistry and Physics*, 16, 5969–5991, <https://doi.org/10.5194/acp-16-5969-2016>, 2016.
- Francisco, M. A. and Krylowksi, J.: Chemistry of Organic Nitrates: Thermal Chemistry of Linear and Branched Organic Nitrates, *Industrial & Engineering Chemistry Research*, 44, 5439–5446, <https://doi.org/10.1021/ie049380d>, 2005.
- 615 Fry, J. L., Draper, D. C., Zarzana, K. J., Campuzano-Jost, P., Day, D. A., Jimenez, J. L., Brown, S. S., Cohen, R. C., Kaser, L., Hansel, A., Cappellin, L., Karl, T., Hodzic Roux, A., Turnipseed, A., Cantrell, C., Lefer, B. L., and Grossberg, N.: Observations of gas- and aerosol-phase organic nitrates at BEACHON-RoMBAS 2011, *Atmospheric Chemistry and Physics*, 13, 8585–8605, <https://doi.org/10.5194/acp-13-8585-2013>, 2013.
- 620 Fry, J. L., Brown, S. S., Middlebrook, A. M., Edwards, P. M., Campuzano-Jost, P., Day, D. A., Jimenez, J. L., Allen, H. M., Ryerson, T. B., Pollack, I., Graus, M., Warneke, C., de Gouw, J. A., Brock, C. A., Gilman, J., Lerner, B. M., Dubé, W. P., Liao, J., and Welti, A.: Secondary organic aerosol (SOA) yields from NO₃ radical + isoprene based on nighttime aircraft power plant plume transects, *Atmospheric Chemistry and Physics*, 18, 11 663–11 682, <https://doi.org/10.5194/acp-18-11663-2018>, 2018.
- Fröhlich, R., Cubison, M. J., Slowik, J. G., Bukowiecki, N., Prévôt, A. S. H., Baltensperger, U., Schneider, J., Kimmel, J. R., Gonin, M., 625 Rohner, U., Worsnop, D. R., and Jayne, J. T.: The ToF-ACSM: a portable aerosol chemical speciation monitor with TOFMS detection, *Atmospheric Measurement Techniques*, 6, 3225–3241, <https://doi.org/10.5194/amt-6-3225-2013>, 2013.
- Gao, L., Song, J., Mohr, C., Huang, W., Vallon, M., Jiang, F., Leisner, T., and Saathoff, H.: Kinetics, SOA yields, and chemical composition of secondary organic aerosol from β -caryophyllene ozonolysis with and without nitrogen oxides between 213 and 313 K, *Atmospheric Chemistry and Physics*, 22, 6001–6020, <https://doi.org/10.5194/acp-22-6001-2022>, 2022.
- 630 Hu, W., Handschy, A., and Jimenez, J. L.: AMS Capture Vaporizer Spectral Database, http://cires1.colorado.edu/jimenez-group/AMSsd_CV/.
- Hu, W., Campuzano-Jost, P., Day, D. A., Croteau, P., Canagaratna, M. R., Jayne, J. T., Worsnop, D. R., and Jimenez, J. L.: Evaluation of the new capture vaporizer for Aerosol Mass Spectrometers (AMS) through laboratory studies of inorganic species, <https://doi.org/10.5194/amt-2016-337>, 2016a.
- 635 Hu, W., Hu, M., Hu, W., Jimenez, J. L., Yuan, B., Chen, W., Wang, M., Wu, Y., Chen, C., Wang, Z., Peng, J., Zeng, L., and Shao, M.: Chemical composition, sources, and aging process of submicron aerosols in Beijing: Contrast between summer and winter, *Journal of Geophysical Research: Atmospheres*, 121, 1955–1977, <https://doi.org/10.1002/2015JD024020>, 2016b.
- Hu, W., Campuzano-Jost, P., Day, D. A., Croteau, P., Canagaratna, M. R., Jayne, J. T., Worsnop, D. R., and Jimenez, J. L.: Evaluation of the new capture vaporizer for aerosol mass spectrometers (AMS) through field studies of inorganic species, *Aerosol Science and Technology*, 640 51, 735–754, <https://doi.org/10.1080/02786826.2017.1296104>, 2017.
- Hu, W., Day, D. A., Campuzano-Jost, P., Nault, B. A., Park, T., Lee, T., Croteau, P., Canagaratna, M. R., Jayne, J. T., Worsnop, D. R., and Jimenez, J. L.: Evaluation of the new capture vaporizer for aerosol mass spectrometers: Characterization of organic aerosol mass spectra, *Aerosol Science and Technology*, 52, 725–739, <https://doi.org/10.1080/02786826.2018.1454584>, 2018a.
- Hu, W., Day, D. A., Campuzano-Jost, P., Nault, B. A., Park, T., Lee, T., Croteau, P., Canagaratna, M. R., Jayne, J. T., 645 Worsnop, D. R., and Jimenez, J. L.: Evaluation of the New Capture Vaporizer for Aerosol Mass Spectrometers (AMS): Elemental Composition and Source Apportionment of Organic Aerosols (OA), *ACS Earth and Space Chemistry*, 2, 410–421, <https://doi.org/10.1021/acsearthspacechem.8b00002>, 2018b.

- Huang, W., Saathoff, H., Shen, X., Ramisetty, R., Leisner, T., and Mohr, C.: Chemical Characterization of Highly Functionalized Organonitrates Contributing to Night-Time Organic Aerosol Mass Loadings and Particle Growth, *Environmental Science & Technology*, 53, 1165–1174, <https://doi.org/10.1021/acs.est.8b05826>, 2019a.
- Huang, W., Saathoff, H., Shen, X., Ramisetty, R., Leisner, T., and Mohr, C.: Seasonal characteristics of organic aerosol chemical composition and volatility in Stuttgart, Germany, *Atmospheric Chemistry and Physics*, 19, 11 687–11 700, <https://doi.org/10.5194/acp-19-11687-2019>, 2019b.
- Jayne, J. T. and Worsnop, D. R.: Particle Capture Device, <https://patents.justia.com/patent/9267869>, 2016.
- Jickells, T., Baker, A. R., Cape, J. N., Cornell, S. E., and Nemitz, E.: The cycling of organic nitrogen through the atmosphere, *Philosophical Transactions of the Royal Society B: Biological Sciences*, 368, 20130 115, <https://doi.org/10.1098/rstb.2013.0115>, 2013.
- Kiendler-Scharr, A., Mensah, A. A., Friese, E., Topping, D., Nemitz, E., Prevot, A. S. H., Äijälä, M., Allan, J., Canonaco, F., Canagaratna, M., Carbone, S., Crippa, M., Dall'Osto, M., Day, D. A., De Carlo, P., Di Marco, C. F., Elbern, H., Eriksson, A., Freney, E., Hao, L., Herrmann, H., Hildebrandt, L., Hillamo, R., Jimenez, J. L., Laaksonen, A., McFiggans, G., Mohr, C., O'Dowd, C., Otjes, R., Ovadnevaite, J., Pandis, S. N., Poulain, L., Schlag, P., Sellegri, K., Swietlicki, E., Tiitta, P., Vermeulen, A., Wahner, A., Worsnop, D., and Wu, H.: Ubiquity of organic nitrates from nighttime chemistry in the European submicron aerosol, *Geophysical Research Letters*, 43, 7735–7744, <https://doi.org/10.1002/2016GL069239>, 2016.
- Lee, B. H., Mohr, C., Lopez-Hilfiker, F. D., Lutz, A., Hallquist, M., Lee, L., Romer, P., Cohen, R. C., Iyer, S., Kurtén, T., Hu, W., Day, D. A., Campuzano-Jost, P., Jimenez, J. L., Xu, L., Ng, N. L., Guo, H., Weber, R. J., Wild, R. J., Brown, S. S., Koss, A., de Gouw, J., Olson, K., Goldstein, A. H., Seco, R., Kim, S., McAvey, K., Shepson, P. B., Starn, T., Baumann, K., Edgerton, E. S., Liu, J., Shilling, J. E., Miller, D. O., Brune, W., Schobesberger, S., D'Ambro, E. L., and Thornton, J. A.: Highly functionalized organic nitrates in the southeast United States: Contribution to secondary organic aerosol and reactive nitrogen budgets, *Proceedings of the National Academy of Sciences*, 113, 1516–1521, <https://doi.org/10.1073/pnas.1508108113>, 2016.
- Liao, H., Adams, P. J., Chung, S. H., Seinfeld, J. H., Mickley, L. J., and Jacob, D. J.: Interactions between tropospheric chemistry and aerosols in a unified general circulation model, *Journal of Geophysical Research: Atmospheres*, 108, <https://doi.org/10.1029/2001JD001260>, 2003.
- Liu, X., Alves Gouveia, D., Henzing, B., Apituley, A., Hensen, A., Van Dinter, D., Huang, R., and Dusek, U.: Aerosol optical properties within the atmospheric boundary layer predicted from ground-based observations compared to Raman lidar retrievals during RITA-2021, *Atmospheric Chemistry and Physics*, 24, 9597–9614, <https://doi.org/10.5194/acp-24-9597-2024>, 2024.
- Lu, Z., Liu, X., Zaveri, R. A., Easter, R. C., Tilmes, S., Emmons, L. K., Vitt, F., Singh, B., Wang, H., Zhang, R., and Rasch, P. J.: Radiative Forcing of Nitrate Aerosols From 1975 to 2010 as Simulated by MOSAIC Module in CESM2-MAM4, *Journal of Geophysical Research: Atmospheres*, 126, e2021JD034 809, <https://doi.org/10.1029/2021JD034809>, 2021.
- Melillo, J. M.: Disruption of the global nitrogen cycle: A grand challenge for the twenty-first century, *Ambio*, 50, 759–763, <https://doi.org/10.1007/s13280-020-01429-2>, 2021.
- Metzger, S.: Gas/aerosol partitioning 2. Global modeling results, *Journal of Geophysical Research*, 107, 4313, <https://doi.org/10.1029/2001JD001103>, 2002.
- Middlebrook, A. M., Bahreini, R., Jimenez, J. L., and Canagaratna, M. R.: Evaluation of Composition-Dependent Collection Efficiencies for the Aerodyne Aerosol Mass Spectrometer using Field Data, *Aerosol Science and Technology*, 46, 258–271, <https://doi.org/10.1080/02786826.2011.620041>, 2012.
- Mohr, C., DeCarlo, P. F., Heringa, M. F., Chirico, R., Slowik, J. G., Richter, R., Reche, C., Alastuey, A., Querol, X., Seco, R., Peñuelas, J., Jiménez, J. L., Crippa, M., Zimmermann, R., Baltensperger, U., and Prévôt, A. S. H.: Identification and quantification of organic aerosol

- from cooking and other sources in Barcelona using aerosol mass spectrometer data, *Atmospheric Chemistry and Physics*, 12, 1649–1665, <https://doi.org/10.5194/acp-12-1649-2012>, 2012.
- 690 Ng, N. L., Herndon, S. C., Trimborn, A., Canagaratna, M. R., Croteau, P. L., Onasch, T. B., Sueper, D., Worsnop, D. R., Zhang, Q., Sun, Y. L., and Jayne, J. T.: An Aerosol Chemical Speciation Monitor (ACSM) for Routine Monitoring of the Composition and Mass Concentrations of Ambient Aerosol, *Aerosol Science and Technology*, 45, 780–794, <https://doi.org/10.1080/02786826.2011.560211>, 2011.
- Ng, N. L., Brown, S. S., Archibald, A. T., Atlas, E., Cohen, R. C., Crowley, J. N., Day, D. A., Donahue, N. M., Fry, J. L., Fuchs, H., Griffin, R. J., Guzman, M. I., Herrmann, H., Hodzic, A., Iinuma, Y., Jimenez, J. L., Kiendler-Scharr, A., Lee, B. H., Luecken, D. J., Mao, J., McLaren, R., Mutzel, A., Osthoff, H. D., Ouyang, B., Picquet-Varrault, B., Platt, U., Pye, H. O. T., Rudich, Y., Schwantes, R. H., Shiraiwa, M., Stutz, J., Thornton, J. A., Tilgner, A., Williams, B. J., and Zaveri, R. A.: Nitrate radicals and biogenic volatile organic compounds: 695 oxidation, mechanisms, and organic aerosol, *Atmospheric Chemistry and Physics*, 17, 2103–2162, <https://doi.org/10.5194/acp-17-2103-2017>, 2017.
- Pandolfi, M., Querol, X., Alastuey, A., Jimenez, J. L., Jorba, O., Day, D., Ortega, A., Cubison, M. J., Comerón, A., Sicard, M., Mohr, C., Prévôt, A. S. H., Minguillón, M. C., Pey, J., Baldasano, J. M., Burkhardt, J. F., Seco, R., Peñuelas, J., Van Drooge, B. L., Artiñano, B., Di Marco, C., Nemitz, E., Schallhart, S., Metzger, A., Hansel, A., Lorente, J., Ng, S., Jayne, J., and Szidat, S.: Effects of sources and 700 meteorology on particulate matter in the Western Mediterranean Basin: An overview of the DAURE campaign, *Journal of Geophysical Research: Atmospheres*, 119, 4978–5010, <https://doi.org/10.1002/2013JD021079>, 2014.
- Paulot, F., Ginoux, P., Cooke, W. F., Donner, L. J., Fan, S., Lin, M.-Y., Mao, J., Naik, V., and Horowitz, L. W.: Sensitivity of nitrate aerosols to ammonia emissions and to nitrate chemistry: implications for present and future nitrate optical depth, *Atmospheric Chemistry and Physics*, 16, 1459–1477, <https://doi.org/10.5194/acp-16-1459-2016>, 2016.
- 705 Pye, H. O. T., Luecken, D. J., Xu, L., Boyd, C. M., Ng, N. L., Baker, K. R., Ayres, B. R., Bash, J. O., Baumann, K., Carter, W. P. L., Edgerton, E., Fry, J. L., Hutzell, W. T., Schwede, D. B., and Shepson, P. B.: Modeling the Current and Future Roles of Particulate Organic Nitrates in the Southeastern United States, *Environmental Science & Technology*, 49, 14 195–14 203, <https://doi.org/10.1021/acs.est.5b03738>, 2015.
- Rodriguez, M. A. and Dabdub, D.: IMAGES-SCAPE2: A modeling study of size- and chemically resolved aerosol thermodynamics in a global chemical transport model, *Journal of Geophysical Research: Atmospheres*, 109, 2003JD003 639, 710 <https://doi.org/10.1029/2003JD003639>, 2004.
- Romer Present, P. S., Zare, A., and Cohen, R. C.: The changing role of organic nitrates in the removal and transport of NO_x, *Atmospheric Chemistry and Physics*, 20, 267–279, <https://doi.org/10.5194/acp-20-267-2020>, 2020.
- Schlag, P., Kiendler-Scharr, A., Blom, M. J., Canonaco, F., Henzing, J. S., Moerman, M., Prévôt, A. S. H., and Holzinger, R.: Aerosol source apportionment from 1-year measurements at the CESAR tower in Cabauw, the Netherlands, *Atmospheric Chemistry and Physics*, 16, 715 8831–8847, <https://doi.org/10.5194/acp-16-8831-2016>, 2016.
- Song, J., Saathoff, H., Gao, L., Gebhardt, R., Jiang, F., Vallon, M., Bauer, J., Norra, S., and Leisner, T.: Variations of PM_{2.5} sources in the context of meteorology and seasonality at an urban street canyon in Southwest Germany, *Atmospheric Environment*, 282, 119 147, <https://doi.org/10.1016/j.atmosenv.2022.119147>, 2022.
- 720 Song, J., Saathoff, H., Jiang, F., Gao, L., Zhang, H., and Leisner, T.: Sources of organic gases and aerosol particles and their roles in nighttime particle growth at a rural forested site in southwest Germany, *Atmospheric Chemistry and Physics*, 24, 6699–6717, <https://doi.org/10.5194/acp-24-6699-2024>, 2024.

- Takeuchi, M. and Ng, N. L.: Chemical composition and hydrolysis of organic nitrate aerosol formed from hydroxyl and nitrate radical oxidation of α -pinene and β -pinene, *Atmospheric Chemistry and Physics*, 19, 12 749–12 766, <https://doi.org/10.5194/acp-19-12749-2019>, 2019.
- 725 Takeuchi, M., Wang, Y., Nault, B. A., Chen, Y., Canagaratna, M. R., and Ng, N. L.: Evaluating the response of the Aerodyne aerosol mass spectrometer to monoterpene- and isoprene-derived organic nitrate standards, *Aerosol Science and Technology*, 58, 1371–1388, <https://doi.org/10.1080/02786826.2024.2389183>, 2024.
- Ulbrich, I. M., Canagaratna, M. R., Zhang, Q., Worsnop, D. R., and Jimenez, J. L.: Interpretation of organic components from Positive Matrix Factorization of aerosol mass spectrometric data, *Atmospheric Chemistry and Physics*, 9, 2891–2918, [https://doi.org/10.5194/acp-9-2891-](https://doi.org/10.5194/acp-9-2891-2009)
730 2009, 2009.
- Vasilakos, P., Russell, A., Weber, R., and Nenes, A.: Understanding nitrate formation in a world with less sulfate, *Atmospheric Chemistry and Physics*, 18, 12 765–12 775, <https://doi.org/10.5194/acp-18-12765-2018>, 2018.
- Williams, L. R., Gonzalez, L. A., Peck, J., Trimborn, D., McInnis, J., Farrar, M. R., Moore, K. D., Jayne, J. T., Robinson, W. A., Lewis, D. K., Onasch, T. B., Canagaratna, M. R., Trimborn, A., Timko, M. T., Magoon, G., Deng, R., Tang, D., De La Rosa Blanco, E., Prévôt,
735 A. S. H., Smith, K. A., and Worsnop, D. R.: Characterization of an aerodynamic lens for transmitting particles greater than 1 micrometer in diameter into the Aerodyne aerosol mass spectrometer, <https://doi.org/10.5194/amtd-6-5033-2013>, 2013.
- Xu, W., Croteau, P., Williams, L., Canagaratna, M., Onasch, T., Cross, E., Zhang, X., Robinson, W., Worsnop, D., and Jayne, J.: Laboratory characterization of an aerosol chemical speciation monitor with PM_{2.5} measurement capability, *Aerosol Science and Technology*, 51, 69–83, <https://doi.org/10.1080/02786826.2016.1241859>, 2017.
- 740 Xu, W., Takeuchi, M., Chen, C., Qiu, Y., Xie, C., Xu, W., Ma, N., Worsnop, D. R., Ng, N. L., and Sun, Y.: Estimation of particulate organic nitrates from thermodenuder–aerosol mass spectrometer measurements in the North China Plain, *Atmospheric Measurement Techniques*, 14, 3693–3705, <https://doi.org/10.5194/amt-14-3693-2021>, 2021.
- Yu, X., Li, Q., Liao, K., Li, Y., Wang, X., Zhou, Y., Liang, Y., and Yu, J. Z.: New measurements reveal a large contribution of nitrogenous molecules to ambient organic aerosol, *npj Climate and Atmospheric Science*, 7, 72, <https://doi.org/10.1038/s41612-024-00620-6>, 2024.
- 745 Zare, A., Romer, P. S., Nguyen, T., Keutsch, F. N., Skog, K., and Cohen, R. C.: A comprehensive organic nitrate chemistry: insights into the lifetime of atmospheric organic nitrates, *Atmospheric Chemistry and Physics*, 18, 15 419–15 436, [https://doi.org/10.5194/acp-18-15419-](https://doi.org/10.5194/acp-18-15419-2018)
2018, 2018.
- Zheng, Y., Cheng, X., Liao, K., Li, Y., Li, Y. J., Huang, R.-J., Hu, W., Liu, Y., Zhu, T., Chen, S., Zeng, L., Worsnop, D. R., and Chen, Q.: Characterization of anthropogenic organic aerosols by TOF-ACSM with the new capture vaporizer, *Atmospheric Measurement Techniques*,
750 13, 2457–2472, <https://doi.org/10.5194/amt-13-2457-2020>, 2020.